SUBAQUEOUS PALEOSEISMOLOGICAL INVESTIGATION IN THE VARVED SEDIMENTS OF KÖYCEĞİZ LAKE (SW ANATOLIA)

A THESIS SUBMITTED TO
THE GRADUATE SCHOOL OF NATURAL AND APPLIED SCIENCES
OF
MIDDLE EAST TECHNICAL UNIVERSITY

BY

AYŞEGÜL DOĞAN

IN PARTIAL FULFILLMENT OF THE REQUIREMENTS
FOR
THE DEGREE OF MASTER OF SCIENCE
IN
GEOLOGICAL ENGINEERING

JANUARY 2023

Approval of the thesis:

SUBAQUEOUS PALEOSEISMOLOGICAL INVESTIGATION IN THE VARVED SEDIMENTS OF KÖYCEĞİZ LAKE (SW ANATOLIA)

submitted by **AYŞEGÜL DOĞAN** in partial fulfillment of the requirements for the degree of **Master of Science** i**n Geological Engineering, Middle East Technical University** by,

Prof. Dr. Halil Kalıpçılar
Dean, Graduate School of **Natural and Applied Sciences** _____

Prof. Dr. Erdin Bozkurt
Head of the Department, **Geological Engineering** _____

Assoc. Prof. Dr. Ulaş Avşar
Supervisor, **Geological Engineering, METU** _____

Examining Committee Members:

Prof. Dr. Erdin Bozkurt
Geological Engineering, METU _____

Assoc. Prof. Dr. Ulaş Avşar
Geological Engineering, METU _____

Prof. Dr. Nuretdin Kaymakcı
Geological Engineering, METU _____

Assoc. Prof. Dr. Erman Özsayın
Geological Engineering, Hacettepe University _____

Assoc. Prof. Dr. Bora Uzel
Geological Engineering, Dokuz Eylül University _____

Date: 25.01.2023

I hereby declare that all information in this document has been obtained and presented in accordance with academic rules and ethical conduct. I also declare that, as required by these rules and conduct, I have fully cited and referenced all material and results that are not original to this work.

Name Last name : Ayşegül, Doğan

Signature :

ABSTRACT

SUBAQUEOUS PALEOSEISMOLOGICAL INVESTIGATION IN THE VARVED SEDIMENTS OF KÖYCEĞİZ LAKE (SW ANATOLIA)

Doğan, Ayşegül
Master of Science, Geological Engineering
Supervisor : Assoc. Prof. Dr. Ulaş Avşar

January 2023, 82 pages

Although on-fault trenching has been the most common paleoseismological technique, the number of lacustrine paleoseismic investigations has considerably increased in the last two decades. Lacustrine paleoseismology research commonly focuses on Mass Wasting Deposits (MWD) and Soft Sediment Deformation Structures (SSDS). Catchment Response (CR), which is defined as temporary amplification of erosion rates in catchments due to strong ground motions, is another sedimentary trace of paleoearthquakes in lakes. This study investigates paleoseismic evidences in varved sediments of Köyceğiz lake along 19 gravity cores with lengths ranging between 98.80 and 138.70 cm. High-resolution elemental profiles together with optical images were obtained by ITRAX micro-XRF scanner. Varve chronology was generated based on both ITRAX optical and XRF data along one core and the other cores were stratigraphically correlated by using Ca/Ti profiles. It is observed that there is no MWDs in the cores although the region has been experienced several noticeable earthquakes during the last ca. 600 years. The CR due to 1959 earthquake is clearly detected in all of the cores as distinct anomalies along the Cr/Ti profiles. However, the CRs due to earthquakes in mid-19th century are observed only in the northern basin of which catchment is significantly bigger than

the one of southern basin. SSDS in Köyceğiz sediments contains faults, intraclast breccia and laminae disturbances. Besides numerous SSDS temporally correlating with the earthquakes in the region, many other SSDS that are not correlating to neither each other nor earthquakes were also detected. This observation implies that earthquakes may not induce SSDS not only at the water/sediment interface but also in the deeper parts of the sequence. It was also found that, in addition to peak ground acceleration (PGA), peak ground displacement (PGD) due to earthquakes may be a controlling factor on the formation of SSDS.

Keywords: Lacustrine paleoseismology, Köyceğiz lake, Soft sediment deformation, ITRAX micro-XRF scanning, Multiple cores.

ÖZ

KÖYCEĞİZ GÖLÜ (GB ANADOLU) VARVLI SEDİMANLARINDA SUALTI PALEOSİSMOLOJİ ARAŞTIRMASI

Doğan, Ayşegül
Yüksek Lisans, Jeoloji Mühendisliği
Tez Yöneticisi: Doç. Dr. Ulaş Avşar

Ocak 2023, 82 sayfa

Fay üzerinde hendek açma, en yaygın paleosismik çalışma yöntemi olmasına karşın son on yılda sualtı paleosismoloji araştırmalarının da sayısı oldukça artmıştır. Göl paleosismolojisi araştırmaları geniş ölçüde kütle hareketi çökelleri (KHÇ) ve yumuşak sediman deformasyon yapılarına (YSDY) odaklanmaktadır. Deprem kaynaklı şiddetli yer sarsıntılarının beslenme alanındaki erozyon miktarını geçici olarak arttırması olarak tanımlanan Beslenme Alanı Tepkisi (BAT) eski depremlerin bir diğer sedimanter izidir. Bu çalışma, uzunlukları 98.80- 138.70 cm arasında değişen 19 adet gravite karot boyunca Köyceğiz Gölü'nün varvlı sedimanlarındaki paleosismik izlerin incelenmesidir. Yüksek çözünürlüklü element profilleri ile optik görüntüler ITRAX mikro-XRF tarayıcısı kullanılarak elde edilmiştir. Varve kronolojisi bir karotun ITRAX optik görüntüsü ve XRF datasına dayanılarak oluşturulmuştur ve diğer karotlar Ca/Ti profilleri kullanılarak stratigrafik olarak deneştirilmiştir. Köyceğiz bölgesinde son 600 yılda kayda değer depremler yaşanmış olmasına rağmen, gölün istifinde KHÇ izine rastlanmamıştır. 1959 depremine ait BAT ise tüm karotların Cr/Ti profillerinde oldukça belirgin anomaliler olarak gözlenmiştir. Ancak 19. yüzyıl ortalarında meydana gelen depremlerin BAT'ları yalnızca beslenme alanı çok daha büyük olan kuzey havzada gözlenmiştir. Köyceğiz

sedimanlarındaki YSDY'ler fayları, intraclast breşleri ve lamina bozukluklarını içermektedir. Zamansal olarak bölgedeki depremler ile deneştirilebilen birçok YSDY'nin yanında, birbiriyle ve de depremler ile uyuşmayan bir çok YSDY de tespit edilmiştir. Bu gözlem depremlerin sadece su/sediman sınırında değil istifin daha derinlerinde de deformasyon yaratabileceğini göstermektedir. Ayrıca, depremlerin ürettiği En Yüksek Yer İvmesi (PGA)'nin yanında, En Yüksek Yer Değiştirme (PGD) değerlerinin de sedimanlardaki YSDY'lerin oluşumunda etkin bir faktör olabileceği bulunmuştur.

Anahtar Kelimeler: Göl paleosismolojisi, Köyceğiz gölü, Yumuşak sediman deformasyonu, ITRAX mikro-XRF taraması, Çoklu karot.

To my family

ACKNOWLEDGMENTS

This study was conducted within the scope of “Köyceğiz Gölü (Muğla) Varvlı Sedimanlarında Sedimanter Deprem Kayıtlarının İncelenmesi” project with project no: 117C021, which was funded by Türkiye Bilimsel ve Teknolojik Araştırma Kurumu (TÜBİTAK).

I would like to express my sincere gratitude to my supervisor, Assoc. Prof. Dr. Ulaş Avşar for his invaluable support, mentorship, and patience throughout this research. I am very thankful for his creative and constructive guidance that brought me new perspectives and taught me the importance of unbiased thinking.

I am very grateful to all jury members, Prof. Dr. Erdin Bozkurt, Prof. Dr. Nuretdin Kaymakçı, Assoc. Prof. Dr. Erman Özsayın , and Assoc. Prof. Dr. Bora Uzel, for taking the time to improve my thesis.

Also, I would like to thank Zeynep Nisan Kaya, Akın Çil, Özlem Karadaş, Zeynep Bektaş, Kaan Onat, and Hakan Bora Okay for their invaluable advice and support throughout the thesis writing process.

I would also like to thank my dearest friends Çağla Karakaş, Neşe Çınar, Seyhun Kılıç, Kerem Ürman, Emre Güngör, Gaye Baştürk, Sertan Eruysal, Cem Üner, Mert İnanç Örge, Serap Şen for their endless supports and motivations.

Finally, I am deeply grateful to my parents, Zaide Doğan and Yalçın Doğan, for their unconditional love, encouragement, supports, and patience not only for this study but throughout my life.

TABLE OF CONTENTS

ABSTRACT v

ÖZ vii

ACKNOWLEDGMENTS x

TABLE OF CONTENTS xi

LIST OF TABLES xiii

LIST OF FIGURES xiv

CHAPTERS

1 INTRODUCTION 1

1.1 Purpose and Scope 20

1.2 Study Area: Köyceğiz Lake 22

2 MATERIALS AND METHODS 27

2.1 Bathymetric Survey and Sediment Coring 27

2.2 Core Splitting and U-Channel Extraction 29

2.3 ITRAX Micro-XRF Core Scanning 30

2.4 Core Chronology 33

2.5 Core-to-core Correlation 34

2.6 Calculation of the Deformation Index 35

2.7 Peak Ground Acceleration (PGA) and Peak Ground Displacement (PGD) 35

3 RESULTS 37

4 DISCUSSION 51

4.1 Seismites 52
4.1.1 Catchment Response (CR) 52
4.1.2 Soft Sediment Deformation Structures (SSDS) 54
4.2 Instantaneous Deposits 59
5 CONCLUSIONS 61
REFERENCES 63
APPENDICES
APPENDIX-1 81
APPENDIX-2 82

LIST OF TABLES

TABLES

Table 1.1. Hierarchical Classification of Paleoseismic Evidence with Examples of Features (modified from McCalpin & Nelson, 2009). 2
Table 2.1. Coordinates and length of 19 cores 29

LIST OF FIGURES

FIGURES

Figure 1.1. Stratigraphic columnar section schematizing lacustrine sedimentary traces of earthquakes (modified from Avşar et al., 2016). 7

Figure 1.2. Bathymetry map with inflow creeks, outflow channel, and locations of 19 cores retrieved from Köyceğiz lake. The location of the study area, catchment topography, and lithology in/ around Köyceğiz Lake are shown in the frame (modified from Avşar et al., 2016). The blue star represents the core studied by Avşar et al. (2016)..... 23

Figure 1.3. The progress of the tear series along the Pliny-Strabo Trench and simplified onland normal faults represented by a conceptual block diagram (Modified from Tosun et al., 2021). 24

Figure 1.4. Instrumental and historical earthquakes and faults around Köyceğiz lake. a) Instrumental earthquake years with given magnitudes (in brackets) and locations (red dots)(BDTİM, 2022). b) Historical earthquake years with estimated magnitudes (in bracket) and uncertainty of epicentral locations (grey and black circles and ellipses) (Albini et al., 2013). Errors in magnitudes of historically recorded earthquakes were given. Onland faults (adopted from active faults map of Emre et al., 2011) and offshore faults (adopted from Sakellariou & Tsampouraki-Kraounaki, 2018)..... 25

Figure 2.1. U-channel extraction process. a) Steps represents u-channel extraction processes. b) Cross-sectional view of processes and dimensions of plastic cable channel. c) Top-view of the processes. 30

Figure 2.2. ITRAX Micro XRF system (Croudace et al., 2006). (1) X-ray tube, (2) radiography, (3) XRF. 31

Figure 3.1. 7 Distinct faults (a-g) observed in optical images of the cores in cm scale. Core numbers and depth of core sections were shown at the bottom corner of the core images. Red arrows indicate the upper termination of the faults. 38

Figure 3.2. 9 Distinct faults (a-i) observed in optical images of the cores in cm scale. Core numbers and depth of core sections were shown at the bottom corner of the core images. Red arrows indicate the upper termination of the faults. 39
Figure 3.3. Intraclast breccias observed in optical images of the cores in cm scale. Boundaries of IB were shown with red brackets, and core numbers and depth values were shown below each core section. 40
Figure 3.4. Disturbed laminations observed in optical images of the cores in cm scale. a) visually distinct DL showed by red bracket. b) vague DL showed by red bracket. Core numbers and depth of core sections were given below each image. 41
Figure 3.5. Absence of carbonaceous laminae in core intervals. Core numbers (top left corner) and depth values (below each core) were given in cm scale..... 42
Figure 3.6. Varve counting of core number 13. White dots indicate counted carbonaceous laminae, and the ages of laminae on 50 years scale were shown on the right side of the core with a given depth in cm 43
Figure 3.7. Varve counting of core number 13. White dots indicate counted carbonaceous laminae, and the ages of laminae on 50 years scale were shown on the right side of the core with a given depth in cm. 44
Figure 3.8. Correlation of optical images from 19 cores (related core numbers were given above each core) shown by 7 horizontal black line with years based on varve counting. Coeval SSDS and instantaneous deposits were correlated with respect to their assigned color as shown in the legend. 46
Figure 3.9. Close-up view of compatibility of 7 visually distinct marker laminae levels of 19 cores. Core numbers were shown top of each core. 7 marker laminae indicated by arrows. 47
Figure 3.10. Correlation of Ca/Ti of 19 cores based on peaks of 7 marker laminae 48
Figure 3.11. Correlation of $(Cr, Ni)_{av}/(Ti, K, Fe)_{av}$ of 19 cores based on 7 marker laminae with respect to depth..... 49
Figure 4.1. Correlation of core numbers 7 and 13 based on Ca/Ti with respect to depth a) Correlation of compatible peak points shown by grey lines. b) Overlapped

view of 7 and 13 after correlation. c) Close-up view of correlated cores between the 40-50 cm. 51
Figure 4.2. Correlation of Ca/Ti profile of 19 cores with respect to time. 52
Figure 4.3. Cr/Ti peaks of correlated 19 cores and their locations in Köyceğiz lake. Blue starts indicate cores studided in Avşar et al. (2016) 53
Figure 4.4. Temporal comparison of DI of 17 cores. The relation of SSDS with known earthquakes were emphasized by dashed lines with given earthquake years. Historical earthquakes were given at the bottom right corner of the figure 56
Figure 4.5. Temporal comparison of median DI profile, overlapped Cr/Ti graphs of both south and north basins cores, Cr/Ti graph of core 11, predicted PGD and PGA calculated by Avşar et al. (2016). Historical earthquakes were given at the bottom right corner of the figure 58
Figure 4.6. Instantaneous deposits. a) Correlated instantaneous deposits (cores 18,19,17,16) and Ca/Ti graph of core 16 (Ca/Ti background trend represented by the thick green line). b) Close-up view of the deposit in core 18. 60

CHAPTER 1

INTRODUCTION

Earthquakes have been one of the most destructive natural disasters throughout history. They have significant impacts on both human lives and the soul of the countries. For instance, in 1999, two earthquakes occurred in Kocaeli (Mw 7.4) and Düzce (Mw 7.2); 18.243 people lost their lives, and around 50.000 people were injured, approximately 380.000 residences and workplaces collapsed or were damaged (BİB, 2002). They may seem just numbers, but they refer loss of families, psychologically devastated societies, and economically disrupted countries. In 2022 another earthquake occurred in Gölyaka, Düzce, with Mw 6.0 and 2 people lost their lives, and 181 buildings were heavily damaged (Özalp & Kürçer, 2022). These decreases in numbers are highly related to precautions taken after the 1999 earthquakes. This is an excellent example of the possibility of reducing the effects of earthquakes by taking necessary precautions based on the results of detailed investigations of the relevant area. Thanks to scientific and technological developments, earthquakes can be examined quantitatively; thus, their traces and magnitudes can be used for suggesting some precautions according to the results. Studying past earthquakes, which is known as paleoseismology, plays an essential role in this respect. Paleoseismology investigations provide detailed information about the size, location, and timing of the paleoearthquakes. Using this knowledge, past earthquakes' behavior and recurrence intervals can be interpreted to analyze the probability and severity of future earthquakes. Past earthquakes leave their traces in sedimentary sequences. These traces were classified hierarchically in McCalpin & Nelson (2009) regarding to genesis, location, and timing formed by past earthquakes (Table 1.1).

Table 1.1. Hierarchical Classification of Paleoseismic Evidence with Examples of Features (modified from McCalpin & Nelson, 2009).

Level 1: Genesis	**Primary (created by tectonic deformation)**			
Level 2: Location	**On-Fault**		**Off-Fault**	
Level 3: Timing	***Instantaneous (coseismic)***	***Delayed Response (postseismic)***	***Instantaneous (coseismic)***	***Delayed Response (postseismic)***
Geomorphic Expression	Fault Scarps Fissures Folds Moletracks Pressure Ridges	Afterslip contributions to features at left Colluvial aprons	Tilted Surfaces Uplifted shorelines Subsided shorelines	Tectonic Alluvial terraces After slip contributions to features at left
Stratigraphic Expression	Faulted strata Folded strata Unconformities or disconformities	Scarp-derived colluvial wedges Fissure fills	Tsunami deposits and erosional unconformities caused by tsunamis	Erosional unconformities and deposits induced by uplift, subsidence and tilting
Abundance of Similar Nonseismic Features	Few	Few	Some	Common
Level 1: Genesis	**Secondary (created by seismic shaking)**			
Level 2: Location	**On-Fault**		**Off-Fault**	
Level 3: Timing	***Instantaneous (coseismic)***	***Delayed Response (postseismic)***	***Instantaneous (coseismic)***	***Delayed Response (postseismic)***
Geomorphic Expression	Sand Blows Landslides and lateral spreads in the fault zone Disturbed trees and tree-throw craters	Retrogressive landslides originating in the fault zone	Sand Blows Landslides and lateral spreads beyond the fault zone Disturbed trees and tree-throw craters Fissures and Sackungen Subsidence from sediment compaction	Retrogressive landslide beyond the fault zone
Stratigraphic Expression	Sand dikes and sills Soft sediment deformation Landslide toe thrust	Sediment deposited from retrogressive landslides	Sand dikes Fillled craters Soft sediment deformation structures (SSDS) Turbidites	Erosion or deposition (change in sedimentation rates) in response to retrogressive landslides or surface features such as fissures. Lateral spreads, or sand blows, or other forms of landscape disturbance
Abundance of Similar Nonseismic Features	Some	Very common	Some	Very common

Genesis classification depends on whether the evidence was created by seismic shaking or tectonic deformation, location indicates whether features formed on-fault or off-fault, and timing is related to the occurrence of traces co-seismically or post-seismically. Tracking these records in the sedimentary deposits is a critical point for paleoseismological research.

Concepts of seismology, structural geology, and tectonics were adjusted in paleoseismology to track earthquake traces (McCalpin & Nelson, 2009). However, the field methods and techniques are obtained from other disciplines such as sedimentology, archaeology, paleoecology, geomorphology, age dating, soil mechanics, photogrammetry, or pedology (McCalpin & Nelson, 2009). Therefore, many techniques can be used in paleoseismology studies, such as on-fault trenching, subaqueous paleoseismology, speleoseismology, dendroseismology, and archaeoseismology.

Tracking past earthquake traces within cave deposits (speleoseismology) focuses on observing the growth direction changes and fractured or broken speleothem to determine the timing of past earthquakes. However, suppose annual banding does not exist; in that case, dating the event will not be appropriate (Becker et al., 2006), and the growth rates of speleothems might be slower than the recurrence interval of the paleoearthquakes that provide incomplete paleoseismological data.

Tree rings (dendroseismology) investigate the sudden change in the ring growth direction and sudden growth interruption caused by damage in the root system. Moreover, decapitation of the tree and sudden increase in growth rate because of inundation or rise in groundwater level due to co-seismic subsidence and cracks in the tree trunk caused by past seismic activities. Although precise dating of past earthquakes can be obtained by dendroseismology, it generally provides short and incomplete records of paleoseismic events based on previous studies (Carver et al., 2004; Jacoby et al., 1997; Meisling & Sieh, 1980).

Archaeoseismology, which is archaeological site investigation, focuses on the past earthquakes' effects on ancient artifacts and human activities, such as damaging of

large buildings, monuments, and their reparations, on-fault displacement of archeological remains, disruption of artificial hydrographic networks, and sudden migration from the region (Caputo and Helly, 2008). Since the archaeoseismological approach includes too many objects to examine, it requires experts from different branches, such as archaeologists, architects, historians, geologists, structural engineers, etc. This creates problems related to merging data provided by these various methodologies used by different branches. Therefore, a compatible interdisciplinary study is crucial to supply complete and precise data if the level of ancient civilization is appropriate to apply archaeoseismological investigation methods. The techniques mentioned above have limitations related to incompleteness and recording short temporal spans, but they can still provide valuable information in paleoseismology research.

On the other hand, on-fault trenching, a more commonly used and better-developed technique, examines surface fault rupturing features directly on fault and thus proves that inspected event is definitely of seismic origin and provides complete and longer records. This technique mainly investigates the on-fault sedimentary sequences to determine earthquake-related event horizons and approximately date these events to obtain the timing of surface fault rupturing using Quaternary dating methods. Although the on-fault trenching technique has more advantages than the others, it has some limitations. One of the limitations is related to erosional processes that can erase earthquake traces that may take place in the trenching site, which will cause misinterpretation of the recurrence interval of paleoearthquakes. Another limitation is related to the magnitude of past earthquakes. Since surface rupturing generally does not take place in case of moderate earthquakes, these types of past earthquake traces cannot be followed by this technique. The other limitation is applying this technique to offshore and blind faults (reverse and thrust faults), which is almost impossible (Avşar, 2013). Moreover, on-fault trenching typically provides an unreliable age probability density function (e.g., Berryman et al., 2012), so earthquake records most probably will be incomplete. For example, overestimating seismic event age may occur while dating charcoal samples collected from the trench

surface due to the time that passed from the formation and absorption of charcoal in the sediments (Bollinger et al., 2016). These obstacles and limitations increase the interest in subaqueous paleoseismology.

Subaqueous paleoseismology investigates the traces of paleoearthquakes in marine and lacustrine sedimentary sequences due to the potential of these environments as having long temporal spans, good preservation, and well spatial coverage. This makes stratigraphic correlation along the source area achievable, which is typically hard to achieve by on-land paleoseismology studies. In addition, past earthquakes that cannot be observed on land due to low to moderate magnitudes that cannot create surface ruptures can be detected by subaqueous paleoseismology studies using high-resolution seismic survey and sediment core analysis and tracing the geochemical and sedimentological anomalies. Lakes are pretty stable depositional environments, so lake sediments are suitable for recording and preserving secondary effects of tectonic activities such as in-situ soft sediment deformations (Strasser et al., 2013a). Since event deposits of paleoearthquakes (seismites) observed in lake sedimentary sequences are occurred due to ground shaking, both intraslab, crustal, and megathrust earthquake traces can be observed in lacustrine environments (Van Daele et al., 2019). Therefore, estimation of the conditional probability of seismic shaking above a certain threshold for a specific region can be done by using lake records (e.g., Howarth et al., 2016; Moernaut, 2020; Rodríguez-Pascua et al., 2010). Limitations of lacustrine paleoseismology are related to erosive processes such as sandy turbidity currents (Hizzett et al., 2018), sliding and slumping (Moernaut et al., 2019), and in-situ deformations (Agnon et al., 2006). These processes may cause the erosion of the older earthquake traces and provide an incomplete paleoseismic archive, which is more likely to occur in regions with low sediment influx and short recurrence intervals of earthquakes. Moreover, some seismites might be masked by other event deposits that occur afterward, which leads to misinterpretation related to the timing and recurrence interval of paleoearthquakes. In addition, paleoclimatic and paleoenvironmental events can also provide similar traces as paleoearthquakes left, so lake paleoseismology investigations require careful examination of these event

deposits and their basin-wide correlation but most importantly temporal correlation between these event deposits and historically and instrumentally recorded earthquakes. Obtaining precise sediment chronology is necessary to correlate events and past earthquakes temporally. Radiocarbon dating can be problematic in subaqueous paleoseismology due to the hard-water effect, similar to on-fault trenching. Still, other alternative radiocarbon sources such as terrestrial macrofossils deposited in the lacustrine basin also might be problematic because of the low abundance in lake sediments and possible reworking and redeposition of these macrofossils (Björck & Wohlfarth, 2005). However, these problems can be overcome because stable depositional conditions of lakes might provide continuous and well-preserved sediment stratigraphy, enabling temporal and spatial correlations between subaquatic sedimentary records. Moreover, suppose climatic and environmental conditions are suitable. In that case, varves (annually deposited laminae) can be formed in lacustrine basins, which is very useful for lacustrine paleoseismology studies since varve sediments allow direct dating of sedimentary sequence (Zolitschka et al., 2015). Basin-wide spatial and temporal correlation of event deposits, which requires multiple cores, provides insight into their formation mechanism since, unlike other event traces, many seismites occur coevally in different parts of the lake. For instance, slope mass failures related to routine overloading depend on sediment influx in the specific slope, so different slopes with different sediment influx amounts and slope angles are unlikely to fail simultaneously. Therefore, these deposits' basin-wide temporal and spatial correlations are generally uncommon. Seismoturbidites, on the other hand, co-occur typically at different locations in the lacustrine environments (e.g., Moernaut et al., 2007; Schnellmann et al., 2006; Waldmann et al., 2011) by the earthquake-generated seismic waves that can affect all basin.

A wide variety of earthquake-triggered deposits and features in lake sediments are utilized in paleoseismic investigations (Figure 1.1). These traces were schematized with respect to their timing (co-seismic, immediate post-seismic, and long-term post-seismic) as stratigraphical columnar section by Avşar (2013) (Figure 1.1).

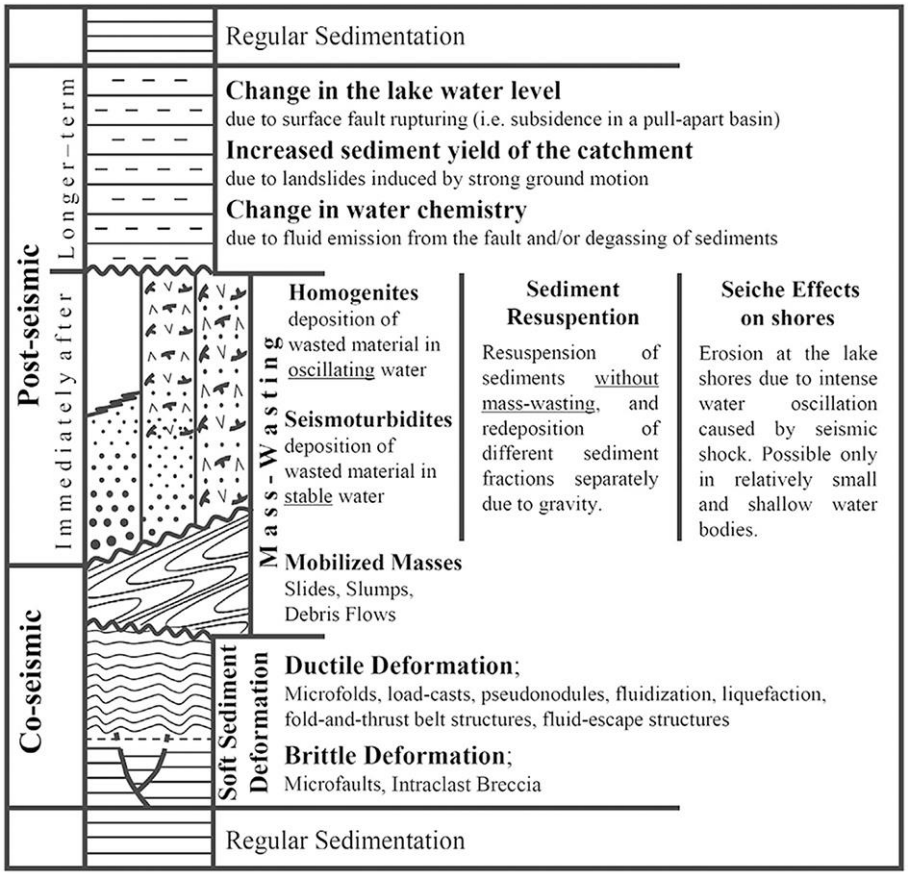

Figure 1.1. Stratigraphic columnar section schematizing lacustrine sedimentary traces of earthquakes (modified from Avşar et al., 2016).

In-situ soft sediment deformations and mass wasting deposits are the most remarkable earthquake traces in subaqueous paleoseismology research (e.g., Goldfinger, 2011; Goldfinger et al., 2003, 2007; Inouchi et al., 1996; McHugh et al., 2016; Moernaut et al., 2014, 2017; Molenaar et al., 2021, 2022; Monecke et al., 2004, 2006; Oswald et al., 2021; Strasser et al., 2013)

Seismic in-situ soft sediment deformation (SSD) is a co-seismic event that can be either brittle (microfaults, intraclast breccias) or ductile (microfolds, fluidization, liquefaction, load-casts, fluid escape structures, pseudonodules and fold, and thrust belt structures) (Avşar et al., 2016).

Fluid escape structures (e.g., water-escape cusps, clastic dykes, pillar structures) are also named liquefaction features or structures (Agnon et al., 2006; Molenaar et al.,

2022; Monecke et al., 2004). Seismically induced liquefaction occurs when pore water pressure increases and the shear strength of saturated, granular, and loose sediments decreases by the effect of seismic shearing, and as a result, water is expelled from sediment. For densely packed sediments, on the other hand, pore water pressure does not increase as much as in loose ones, and loss in strength is also relatively more minor, so they are less prone to be affected by the liquefaction process (Allen, 1982; Owen, 1987; Owen & Moretti, 2011). Overburden pressure is another limitation of liquefaction processes since it is asserted most liquefaction processes occur in sediments located in less than 5 m depth (Obermeier, 1996; Owen & Moretti, 2011). When flowing water exerts adequate vertical force through a cohesionless sediment layer, rapid dilatation of the layer occurs, and grain-to-grain support turns into fluid support, which leads to fluidization. Unlike liquefaction, fluidization is claimed to generally occur in silt and mud-rich layers with minimal amounts of clay (almost cohesionless) (Lowe, 1975). Fluid escape structures are formed by unstable fluidization and/or liquefaction processes (e.g., Allen, 1982; Moretti & Sabato, 2007; Nichols et al., 1994; Owen & Moretti, 2011)

Intraclast breccia is one of the liquefaction features formed by ground shaking that leads to mechanical instability and disruption in the sediments and oscillation of the water column. This causes the pore water pressure of the sediments to overcome the confining pressure of overlying lake water (liquefaction of sediments) and escape from uncompacted sediments. When pore water pressure overcomes the cohesive stress between originally laminated particles, cracks and step-like topography (microfaults) might be formed (Agnon et al., 2006). If it cannot surpass the cohesive stress, folds and undulations might probably occur in the cohesive laminae. Sediments deposited at the water-sediment interface become suspended when the drag force created by fluid escaping from the sediment is bigger than the gravitational force and momentum of seiche triggered by seismic waves. This incident keeps them suspended; later, this suspended clast that was previously part of laminae deposited gradually when the seiche effect weakened and stopped. Afterward, this deposited layer, called intraclast breccia (IB), is formed and covered by background sediments

(Agnon et al., 2006). Various authors generally linked earthquake-related brittle, soft-sediment deformation structures (faults) with earthquake-triggered liquefaction that leads to fractures in coherent layers (e.g., Becker et al., 2006; Ringrose, 1989; Seilacher, 1969), but these observed faults were larger than microfaults. In Monecke et al., (2004), normal microfaults with 2 cm long and 1-2 mm displacement were observed in finely laminated carbonate-rich layers, and the occurrence of these microfolds was linked with the relatively fast lithification-driven strengthening of these layers that caused an increase in the tendency to be fractured by seismic shaking. Load structures (e.g., pseudonodules, load casts) are formed due to density contrast between two sediment layers when they are still soft, and denser sediment must be deposited on top of lighter ones (Owen, 2003) to provide a basis for load structure formation. Deposition of denser material on top of the lighter one is considered to be occurring due to earthquake-induced liquefaction processes, and the sinking of denser uplifted layers leads to load cast formation when part of these denser materials pinches off pseudonodules are formed (Shanmugam, 2017). In addition, the direct effect of earthquake-driven disturbance can also lead to the occurrence of load structures. Intraclast breccia (IB) might also be formed directly by earthquake seismic shear energy. IB formation is claimed to depend on sediments characteristic (e.g., rheology, size, composition) and layer thickness, which have strong control on layers in terms of deformation mechanisms (e.g., clay-dominated clastic strata are claimed as less prone to be deformed by earthquake-induced liquefaction/fluidization processes than strain softening (Nichols et al., 1994). Slope angle and the existence of basal shear surface are also asserted as controlling factors (Molenaar et al., 2022). Therefore, to assign earthquake-induced liquefaction as the formation mechanism for SSDS features related to liquefaction and/or fluidization (e.g., water-escape cusps, pillar-like structures) are required to be observed below the deformed layer (Owen & Moretti, 2011). If these features are not very identifiable (e.g., related load cast structure might deform liquefaction and/or fluidization imprints), sediment properties should be carefully examined. As in the case of above mentioned SSDS (load structures, microfaults, IB), there exist several SSDS

formation processes triggered by earthquakes. The earthquake-triggered liquefaction/fluidization was asserted as one of them (e.g., Agnon et al., 2006; Allen, 1982; Moretti & Sabato, 2007; Nichols et al., 1994; Owen & Moretti, 2011). Another one is claimed to be related to Kelvin- Helmholtz instability (KHI) (e.g., Heifetz et al., 2005; Molenaar et al., 2022; Wetzler et al., 2010). Generated SSDS by KHI mechanism (folds, disturbed laminations, intraclast breccias) was suggested that it is directly related to earthquake shear seismic energy. Suppose this energy can overcome the gravitational potential energy of stably stratified sediments. In that case, the contrast between layers that is probably related to lithological and physical properties (e.g., layer thickness, the abundance of cohesive minerals) leads to shearing at layer boundaries, thereby inducing deformation (Heifetz et al., 2005; Wetzler et al., 2010). The stability of these two beds was suggested to be disrupted by shear-driven rotational movement and denser layer uplifts above the lighter layers and form wavy structures. The uplifted denser layer is prone to collapse into lighter one, leading to billow vortices forming. If the effects of shearing continue, the mixing of these two layers will occur due to secondary shear developed by differential movement of vortices regarding the lithological and physical differences and leads to the formation of intraclast breccia (Heifetz et al., 2005; Wetzler et al., 2010). Therefore, disturbed lamination and folds do not present any breakaway of individual laminations that they formed on but show undulation and clear vergence, respectively.

On the other hand, Intraclast breccias consist of clasts of laminations, partly homogenized, and mixed deformed sediments. Important parameters that might have control on SSDS formation, in addition to lithology and physical properties of layers, are basal shear surface effect (depending on the existence and properties of clastic sediments), slope angle, and seismic shaking strength (e.g., intensity, peak ground acceleration) (Molenaar et al., 2022). In Molenaar et al. (2022), these parameters and their effects on Kelvin-Helmholtz instability-related SSDS characteristics (deformation degree and thickness) in lake Rinihue biogenic varve sequences have been investigated by using 17 sediment cores taken from slope angles approximately

ranging from 0.2º to 4.9º. Within the varve sequence, there exists volcanogenic fine- and coarse-grained (e.g., lahar and tephra, respectively) deposits, which are suitable to create basal shear by strain softening (fine-grained volcanogenic deposits) and liquefaction (coarse-grained volcanogenic deposits), induced by earthquake. SSDS are mostly (72%) observed directly on top of these deposits. Moreover, water film formation related to dewatering both fine- and coarse-grained volcanogenic deposits concentrates the strain between the basal shear surface and overlying background, thereby preventing the incorporation of the basal shear surface into the formation of SSDS. Slope angle has the highest control on the deformation thickness, and slope angle is supported by the depth of volcanogenic deposits and shaking strength (peak ground acceleration (PGA) in that study). A higher slope angle has higher gravitational downslope stress, so sediments deposited on a higher slope angle are more prone to be affected by earthquake-induced shear stress and deformation. Although they could not find a direct relation between PGA and deformation thickness, data showed that in the low slope angle (<1º) maximum, the highest seismic shaking strength and the stratigraphic depth of volcanogenic deposits constructed the highest possible deformation thickness. Deformation degree and spatial distribution of deformation, on the other hand, are first-order regulated by PGA regarding this observation. The thickness of the layer that undergoes deformation has secondary controls on the deformation degree. The thinner sequence undergoes higher shear seismic energy density, which leads higher deformation degree even at a lower slope angle (i.e., <1º). Sediment composition might influence the deformation degree (e.g., diatom, in this study, might lower the propensity of sediments to deformation.).

Other than the co-seismic effects of earthquakes, there are other SSDS formation mechanisms, such as large-scale slumps and slides that lead to sudden overloading (Schnellmann et al., 2005), overloading by abrupt sediment deposition (Moretti et al., 2001; Moretti & Sabato, 2007; Oliveira et al., 2009), loading by storm-wave action (Alfaro et al., 2002; Molina et al., 1998), large-scale change in water level (Allen,1982) and deformation due to coring procedure (Lotter et al., 1997).

Assigning earthquake seismic shaking as SSDS formation mechanisms to confidently investigate these events with a subaqueous paleoseismological approach is important. To distinguish other triggering mechanisms from earthquake seismic activity, multi-coring from distinct parts of the lake basin or additional coring from different lakes should be applied to test coevality. Suppose observed SSDS in different parts of the lake and even in different lakes is proved to belong to the same chronostratigraphic level. In that case, it will eliminate the possibility of sudden overloading (e.g., by slides/slumps) and rapid deposition (e.g., by flood). Knowing the depth of SSDS will help to rule out storm-wave action since it is ineffective under wave base. The deformation related to the coring procedure can be overcome by applying the suitable coring technique, which will also be effective in avoiding any disturbance and loss of the water-sediment interface (e.g., unlikely piston corer with catcher, which is more likely to disturb water-sediment interface, gravity core generally protects water-sediment interface). Nevertheless, there might still be a disturbance on top of core sediments, so the core top should be carefully examined. If any disturbance is observed, the procedure should be applied again. There are some other possible deformations generated by coring, such as microfaults related to pressure change, regarding the applied coring-driven sinkage of the gas cracks. Consequently, a multi-coring investigation is useful in this sense since sinkage of sediments related to gas crack is unlikely to occur at the same chronostratigraphic level throughout the basin. In addition to the multi-coring approach, temporally correlating these deformations with historically and instrumentally well-known earthquakes, which requires precise core sediment chronology, provides reliable information to assign earthquake seismic shaking as the triggering mechanism of SSDS formation (Fanetti et al., 2008). The importance of obtaining precise sediment chronology becomes clear at this point.

Varve counting, radiocarbon dating, dating of short-lived radionuclides, and paleomagnetic dating are potential dating methods that can generate precise core chronology of lake sediments. Dating of lake sediments via paleomagnetism is simply related to the alignment of magnetic minerals with respect to the declination

and inclination of the magnetic field of Earth during deposition. In the lacustrine environment, comparing the change in the alignment of magnetic minerals with a dated reference curve can provide sediment chronology(Ojala & Tiljander, 2003). However, intensities of the geomagnetic field do not completely comparable with remnant magnetization intensity since sedimentological effects such as grain size distribution and accumulation of magnetic minerals have great control while recording geomagnetic field intensity (Turner & Thompson, 1981). Radiocarbon dating depends on decay processes of ^{14}C within fossil organic matter. Organisms use carbon atoms for building their tissue or photosynthesis, which is in isotopic equilibrium with their habitat (e.g., ocean, saline water) until they die (Björck & Wohlfarth, 2002). Therefore, measuring the decay level of ^{14}C within fossil organic matter with respect to its half-life (5568 years) (Mook, 1986) will approximately give the time of death. The possible problems related to radiocarbon dating are unstable atmospheric ^{14}C production, hardwater effect (e.g., Doran et al., 1999; Hajdas et al., 1993; Shotton, 1972), the reworking of terrestrial radiocarbon source materials (Björck & Wohlfarth, 2005), and relatively hard sample preparation. These problems are more likely to create uncertainty related to the age-depth model. Due to fossil fuel usage and nuclear weapon testing, the variation of 14C in the atmosphere makes it hard to apply the radiocarbon dating method to date the last few hundred years' sediments. To manage this limitation, ^{137}Cs and ^{210}Pb radionuclide dating can be applied to upper-most sediments since ^{210}Pb has a relatively short half-life (22.3 years) and ^{137}Cs was artificially produced radionuclide during the 1953-1963 nuclear weapon test and the 1986 Chernobyl disaster. These two methods precisely date recent sediments and thus can be used to support other dating techniques. For example, even though among these possible dating methods, the most precise one is counting the annually laminated sediments (varve counting), laminae might not be deposited annually, so ^{137}Cs and ^{210}Pb age dating methods can be applied to recent sediments to observe whether laminated sediments represent annual deposition or not (Avşar et al., 2016). After confidently assigning varve to observed sediment layers, direct dating of the sedimentary sequence becomes

achievable by downcore counting of annually deposited laminae. Varve counting may be interrupted by varve mixing, which mainly occurs due to bioturbation, but it is unlikely in lake environments with hostile bottom conditions (e.g., anoxic). Moreover, mixing and disturbance might occur due to seismic activity and other natural phenomena. These two possibilities can be distinguished from each other by the above-stated ways. Unlike homogenous sediment deposits, disturbance of varve sediments due to earthquake seismic activity provides a perfect high-resolution trace of paleoearthquakes since contrast (e.g., in the sense of color and grain size) between seasonally deposited laminae enables to observe of deformations clearly, especially for SSDS. A possible limitation related to the real timing of deformation arises from the occurrence way of SSD because dated deformed sediments might appear to be older than the earthquake event because SSD may occur on sediments that have already been deposited (below the water-sediment interface). On the other hand, if deformation took place at the water-sediment interface simultaneously with earthquake seismic shock, the top part of deformation within the stratigraphic horizon will provide the exact timing of the earthquake event (Avşar et al., 2016). Varve sediments can most probably be served as a reliable source of assigning earthquakes as deformation mechanism by easily comparing the timing of paleoearthquakes and related deformed varve sediments (expected SSDS occurrence on the water-sediment interface can be tested), especially via multiple core investigation approach by carefully correlating them.

Mass wasting deposits which are another important lacustrine earthquake trace (e.g., Chapron et al., 1999; Daxer et al., 2022; Moernaut et al., 2017; Molenaar et al., 2021; Schnellmann et al., 2006) consist of mobilized masses (slides, slumps, debris flow), seismoturbidites, homogenites, sediment resuspension and seiche effects on shores. The product of mobilized masses is commonly called as mass transport deposits (MTD).

Mobilizing and transporting large volumes of sediments from subaquatic slopes to deep basins are known as subaqueous mass movements (e.g., slumps, slides, mudflow), which are quite common processes in both marine and lacustrine

environments (e.g., Masson et al., 2006; Sammartini et al., 2019; Strasser et al., 2013b; Urgeles & Camerlenghi, 2013). Seismic shaking of an earthquake can provide lacustrine slope instability and raise pore water pressure by creating shear stress that leads to the movement of sedimentary sequence deposited on the lacustrine slope. Deposition of these large volumes of mobilized sediments via slides, slumps, and debris flow at the foot of basin slopes is called mass transport deposits (MTD) (Daxer et al., 2020; Sammartini et al., 2019). Moreover, when this earthquake triggered mobilized mass is deposited at distal sites by the effect of turbidity currents created by dilution of moving mass is called seismoturbidites or homogenites (e.g., Bertrand et al., 2008; Chapron et al., 1999; Monecke et al., 2006). The main difference between homogenites and seismoturbidites is that seismoturbidites originated under still water conditions, leading to fining upward deposition when the turbidity currents effect ceases. While homogenites are formed when seismically induced oscillation takes place, which keeps resuspended fine-grained sediments in suspension; when it stops, fine-grained sediments settle and produce homogenites (Beck, 2009; Bertrand et al., 2008; Chapron et al., 1999; Monecke et al., 2006). Besides earthquake triggering, some other triggering mechanisms might lead to the formation of MTD and turbidites. These are continuous sediment loading and increase in subaqueous slope angle, lake water level oscillation, storm wave action, excessive flood events, volcanic eruptions, and hyperpycnal flows. Therefore, a detailed investigation is necessary to distinguish the main triggering mechanism of the mass movements and related turbidity currents; otherwise, misinterpretation will lead the study to deviate from its aim. Fortunately, these mechanisms can be distinguished from earthquake triggering based on their geochemical signatures, grain-size distribution, initiation location of movement, and coevality of deposited features. For instance, hyperpycnal flow deposits that might be induced by flood exhibit lateral grading unlikely to turbidites that show finning upward sequence stratigraphy. Moreover, seismoturbidites and flood-induced turbidites can be distinguished with respect to their sorting (generally, seismoturbidites are poorly sorted), basal grain size (fining upwards of

seismoturbidites), basal erosional contact (reworked background sediment fragments in the base of seismoturbidites), and thickness (since earthquake-triggered turbidity currents are short-lived and have higher energy it has lower thickness), (Vandekerkhove et al., 2020, and references therein). On the other hand, storm wave loading and water level fluctuation, which are the typical triggering mechanism of shallow lakes, can be eliminated by controlling the initiation depth of mass movement, whether it is deeper than the lake fluctuation level and wave base depth or not (Avşar et al., 2014). However, the most important criteria to distinguish mass wasting deposits triggered by the earthquake from other triggering mechanisms is the coevality and synchronicity of deposits and their correlation with historically and instrumentally recorded earthquakes.

Essentially, two methods should be applied to examine coevality and synchronicity: sedimentological examination and test for synchronous triggering, as claimed by Goldfinger (2011). The synchronous test must be applied to make stratigraphic and chronologic correlations. To apply this test, multiple cores are required because seismic waves can trigger multiple turbidity currents and mass failures in a wide area synchronously. In addition, the confluence test also provides useful information since it requires observation of the same number of turbidites occurrence both above and below the confluences. Stratigraphic correlation consists of lithostratigraphic and physical properties correlation, seismic stratigraphic correlation, and assessment of these two methods. While correlating lithostratigraphic and physical properties of sediments, some techniques are very beneficial, such as ITRAX micro-XRF core scanning, grain size analysis, and magnetic susceptibility. Seismic stratigraphic correlation requires a seismic profile of the regarding area and correlation of those profiles. In the evaluation part, it is suggested to make use of remarkable and visible features of the core, mathematically represented results, and correlation coefficients (Goldfinger, 2011). Also, the mineralogical and sedimentological characteristics of the cores should be investigated carefully. Chronologic and stratigraphic correlation of cores can supply valuable information about the mechanism. However, correlating them with instrumentally and historically documented earthquakes will provide more

reliable and accurate results. To achieve the goals mentioned above, precise age dating is a must. The same age dating techniques as mentioned in the SSDS part can be applied to gain accurate sediment core chronology, which can be used to correlate these event deposits with well-known historical earthquakes. Mass-wasting event-based paleoseismology investigations may provide incomplete records since some threshold parameters and conditions should be satisfied to form these event deposits. One of the conditions is related to the sedimentation rate and recurrence interval of seismic activity. The sedimentation rate should be high enough to reproduce slope sequence that tends to fail by the effect of following earthquake or earthquake recurrence interval should be sufficient to enable adequate sedimentation that is prone to failure. The accuracy of the slope angle is another factor. It must be high enough to susceptible to failure (approximately 6 degrees) (Moernaut, 2010).

Sediment resuspension can be originated by seiche or water oscillation effects driven by earthquake seismic activity other than mass-wasting event impact at the water-sediment interface of the steeper part of the lake basin. The resuspended very soft clay-free sediments due to seiche, or water oscillation, consists of organic matter and clastic material that is settled with respect to their density differences (e.g., organic-rich layer underlain by silty layer) in distal lakesides (Avşar et al., 2014; Doig, 1990, 1991, 1998b, 1998a). The deposition thickness of seiche-related sediments is claimed to be thinner than mass-wasting deposits since seiche-related resuspended sediments are soft sediments at the water-sediment interface the amount of these materials is supposed to be less than mass-wasting originated materials amount (Avşar, 2013).

In small and shallow lakes, earthquake-induced water oscillation might have higher energy than in deep and big lakes. It can even rip, rework, and resuspend sediments from the lakes' littoral zone. Deposited sediments at the littoral zone are generally coarse and heavy. Still, decomposed organic matter is light enough to be carried by wind and wave transportation agents throughout the lake, so the traces of the seiche effect can be observed on the basin-wide scale (Avşar et al., 2014).

Catchment response, a longer-term post-seismic event of earthquakes, is another significant trace of paleoearthquakes to track in lacustrine paleoseismology investigations. Since earthquake-triggered landslide and rock fragmentation cause the obvious change in size, petrography, and volume of terrigenous sediment influx from the lake's catchment to the lake (Avşar et al., 2016; Howarth et al., 2012, 2014, 2016; Leroy et al., 2010). Catchment response (CR) is a relatively new concept in lacustrine paleoseismology literature, but there were several observations related to the increase in sediment accumulation in river systems quantitatively. For instance, after the 1999 Chi-Chi Taiwan earthquake (Mw 7.6) amount of suspended sediment was 3-7 times more than in the preseismic period for approximately six years (Dadson et al., 2004; Hovius et al., 2011; Yanites et al., 2010). Another observation was done after the 2008 Wenchuan earthquake (Mw 7.9). This study's result provides the same quantitative data as the 1999 Chi-Chi earthquake related to increased suspended sediment amount. However, the time it took for Longmen Shan river to turn into its original sediment concentration is much wider (from 1.2 ± 0.9 years to 90 ± 65 years) (Wang et al., 2015). In historical archives based upon eyewitness expressions, the term muddy river takes place after large paleoearthquakes (Ambraseys, 2009), which is most probably related to the earthquake-triggered landslide and shattering of rocks that raises erosion rate in catchments, nowadays called as CR. The intensity of sediment influx to the lake with respect to CR is probably dependent on slope angle, type of rock in the catchment, climatic conditions of the studied region, size and amount of streams that feed the lake, earthquake magnitudes, and distance from the research location. The relationship between earthquake magnitude and total volume of the landslide has been studied (e.g., Avşar, 2013; Bommer & Rodríguez, 2002; Keefer, 1984a, 1994; Malamud et al., 2004; Rodríguez et al., 1999) and high correlation ratio (r^2=0.88) was established (Keefer, 1994). In addition, based on a comparison of 52 lakes' catchment areas, lake area ratios done by Avşar et al. (2014) claimed that lakes with relatively larger catchment areas might be more prone to recording earthquake-triggered CR in their sedimentary sequences. In order to examine traces of earthquake-triggered CR lithology of

catchment should be well-known because the change in detrital incoming sediment composition is highly dependent on weathered and eroded sediments from these lithologies. For example, based on paleoseismic investigation of Yeniçağ lake with ultramafic-mafic rock-dominated catchment lithology, post-seismic event deposits show higher-grained siliciclastic materials are enriched in Cr and Ni elements, which represent the weathering products of catchment lithology (Avşar et al., 2014). After the 1959 earthquake with Mw 5.9 around Köyceğiz lake, with peridotite-dominated catchment lithology, post-seismic event deposits that were classified as CR showed similar signals related to Cr and Ni peaks.

Another longer-term post-seismic impact of the earthquake is lake water level change due to co-seismic subsidence, which generally drives a few meters deepening in pull-apart like tectonically controlled basins (Avşar, 2013). A close proximal area of the lake is suddenly submerged by the effect of this event. Shallow water lake environments are more prone to record evidence of this few meters deepening since they are more susceptible to water level fluctuations. Successive subsidence of the basin can be observed in sedimentary sequence as alternating peat and mud layers. Traces of this event can also be tracked by investigating the change in biogeochemical and taxonomical characteristics of diatom, foraminifera, pollen, and organic matter content (Bertrand et al., 2011; Leroy et al., 2009, 2010; Mirecki, 1996; Vologina et al., 2010). For instance, back-wash of sudden inundation might lead to a change in the origin of organic matter content (increase in terrestrial origin organic matter).

Fluid emission from fault and degassing of sediments are claimed to be changing water chemistry based on historical records and eyewitnesses' allegations (Ben-Menahem, 1976). Observation related to this event is very rare in literature. To exemplify, one week before the 1943 earthquake, close to the Dead Sea shore, a new spring was claimed to be appeared and spread white material into seawater for approximately 5 months. In Dead Sea sedimentary sequences, there observed white layers, which were claimed as evidence of paleoseismic events (Ben-Menahem, 1976). However, investigation related to fluid emission is not common in the

literature. Longer term post seismic event deposits of earthquakes are hard to distinguish from paleoclimatic and paleoenvironmental event deposits, so relatively more detailed sedimentological examinations and precise age dating to obtain reliable chronology are a must. Moreover, long historical earthquake records are very valuable in the sense of the reliability of the origin of event deposits.

In light of the aforementioned information, Köyceğiz lake, with varve sediments, offers significant opportunities regarding paleoseismological investigations. It has two basins, northern and southern, with different characteristics. While three inflows feed the northern basin, the southern basin is discharged by the Dalyan channel and fed by very small Sultaniye creeks. The northern basin is relatively straight and shallow (approximately 1.5 degrees, 26 m depth). In contrast, the southern basin is relatively deeper (32 m) and steeper (approximately 5 degrees). Thus, cores taken from these two basins will probably provide an opportunity to observe the effect of these contrasts on traces of past earthquakes as claimed in the (e.g., Moernaut et al., 2017; Molenaar et al., 2021, 2022). Moreover, annually laminated lake sediments lead the construction of precise core chronology and direct dating of event deposits to confidently identify them as seismites by easily and precisely correlating them with historically and instrumentally documented earthquakes.

1.1 Purpose and Scope

The main aim of this study is, by using lacustrine paleoseismology investigation techniques, track the instrumentally and historically well-documented past earthquake traces and understand their relations with each other in the varved sediments of Köyceğiz Lake.

Köyceğiz lake sediments were previously investigated in a paleoseismological approach by Avşar et al. (2016). That study was on a single core retrieved from the southern basin. Earthquake imprints observed in this core were CR and SSDS (faults and laminae disturbance), but no turbidite was found. The relation of these seismites with the magnitude versus epicentral distance of paleoearthquakes was evaluated. In

that study, the PGA threshold was determined for SSDS and CR as 20 and 70 cm/s^2, respectively. It was claimed by Avşar et al. (2016) that most of the SSDS observed in that core formed at the water-sediment interface due to their temporal compatibility with past earthquakes. However, in 2004 and 1806, there is no earthquake record, but SSDSs were observed (Avşar et al., 2016). The possible explanations for this observation are a coring-related disturbance, a change in climatic factors, or an undocumented, relatively low-magnitude local earthquake. One of the most outstanding things about that study is that turbidites were not observed even though many strong earthquakes have affected the lake for the last 500 years. Another one is that soft-sediment deformation intensity does not seem consistent with PGA on some levels (e.g., the 1869 earthquake, even though its epicentral location uncertainty is relatively lower).

The motivation behind this study is to improve the results provided by Avşar et al. (2016) via the multiple cores retrieved from both southern and northern basins. For instance, whether SSDS and CRs' formed coevally throughout the Köyceğiz lake. In addition, to test the threshold values of SSDS and CR within two basins with different characteristics (e.g., slope angle, catchment area) and enhance the number of observations. Moreover, multiple cores provide an opportunity to investigate controlling factors of turbidite formation (e.g., slope angle, sediment influx). The uncertainty of epicentral locations of historical earthquakes (e.g., moderate earthquakes in 1660 and 1871 and strong earthquake in 1741) is another motivation since the earthquake in 1660 left traces in Köyceğiz sedimentary sequence. It is worth tracking traces of the other historical earthquakes with epicentral uncertainty to evaluate their distances better by investigating multiple cores. Multiple cores also might enable us to explain the formation processes of 2004 and 1806 SSDSs.

Nineteen cores (13 from the southern and 6 from the northern basin) were retrieved from Köyceğiz lake to investigate seismites (e.g., SSDS, CR) in more detail within the scope of this study. Cores were examined by ITRAX-Micro XRF core scanner and radiographic imaging, and core chronology was obtained by varve counting.

1.2 Study Area: Köyceğiz Lake

Köyceğiz Lake, whose area is 53 $km^{2,}$ is located in the Muğla province of Southwestern Turkey (Figure 1.2). The lake consists of the Köyceğiz basin in the northern and Sultaniye basin in the southern (Kazanci et al., 1992), with a maximum depth of 26 and 32 meters, respectively found in a bathymetric survey performed in 2014 (Avşar et al., 2016). Köyceğiz Lake is fed by three main creeks named Yuvarlak, Namnam, and Köyceğiz through the northern basin and discharged into the Mediterranean by the Dalyan channel from the southern basin. Mediterranean climate (mild and wet winters and dry and hot summers) is dominant climate in the region. It was discovered that Köyceğiz lake consists of two hydrochemically distinct water layers, the border of which is 10 meters below the water's surface.The bottom water of the lake is permanently anoxic, which leads to classifying Köyceğiz lake as a meromictic lake (anoxic lake bottom) (Bayarı et al., 1995; Kazanci et al., 1992). The catchment area of the lake is 875 km^2 with a maximum of 2200 meters of elevation, dominated by peridotite, which covers approximately 60% of it (Avşar et al., 2016). The research of interest area is standing on Lycian Nappes composed of three main units:eşilbayrak Nappe, Carbonate Nappes (Gülbahar, Tavas, Bodrum Nappes), and Marmaris Nappe from bottom to top (Şenel, 1997). Yeşilbayrak Nappe overlies Beydağları autochthon, which is the base rock of the region and is overlain by Carbonate units consisting of shales and sandstones. The Lower Cretaceous Marmaris Nappe, composed of peridotite, over all other units in the area (Kurtuluş et al., 2019). Köyceğiz Lake is one of Turkey's three lakes representing yearly deposited laminae (varve sediment). The varve deposition in the lake representing one year consists of alternating summer season depositions as yellow-colored laminae rich in carbonate and autumn and winter season depositions as dark-colored laminae rich in clastic and organic matter.

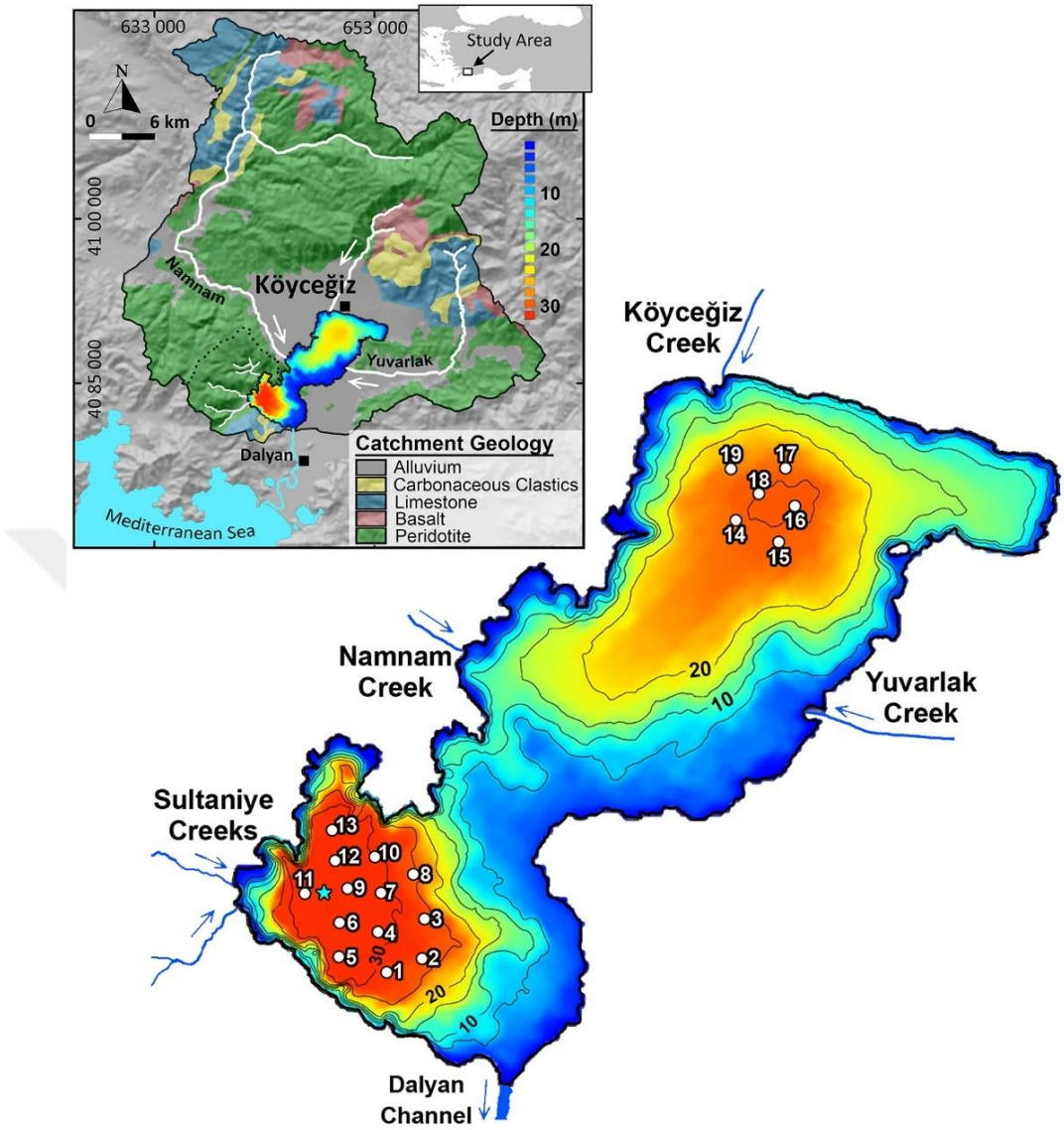

Figure 1.2. Bathymetry map with inflow creeks, outflow channel, and locations of 19 cores retrieved from Köyceğiz lake. The location of the study area, catchment topography, and lithology in/ around Köyceğiz Lake are shown in the frame (modified from Avşar et al., 2016). The blue star represents the core studied by Avşar et al. (2016)

The lake is approximately 30 km west of the northernmost off-shore extension of the Pliny-Strabo trenches. The region is dominated by multi-directional extensional deformation manifested by normal faults onshore and immediate offshore areas (Tosun et al., 2021). In addition, it is also claimed that the strike-slip faults related to the Pliny-Strabo trench do not extend onshore areas (Figure 1.3). They terminate

around the shoreline. Previously Fethiye Burdur Fault Zone was believed to be an onland continuation of the Pliny-Strabo trench that offset the Hellenic and Cyprus arcs sinistrally (Hall et al., 2014). Nevertheless, both Hall et al. (2014) and Tosun et al. (2021) imply that Köyceğiz Lake is located at a very key area to unravel seismic history of the region.

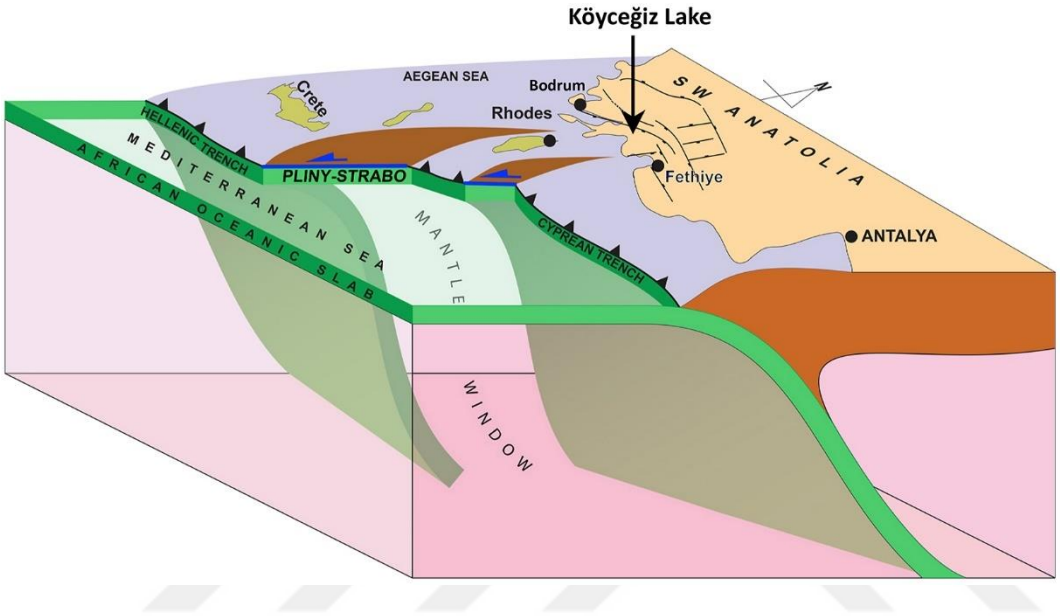

Figure 1.3. The progress of the tear series along the Pliny-Strabo Trench and simplified onland normal faults represented by a conceptual block diagram (Modified from Tosun et al., 2021).

Seismic activities recorded instrumentally during the last century consist of 14 events possibly affecting the lake and its surroundings (BDTİM, 2022). This implication is done with respect to information about the magnitude and approximate distance from the epicenter to the coring location of these 14 past earthquakes (Figure 1.4 a). The magnitudes of the closest earthquakes (1960, 1959, 1956, and 1920) to the lake are relatively weaker than distant ones (1957, 1941, 1926) (Figure 1.4 a). In addition, many historical earthquakes (17) around the study site, are documented by The European Archive of Historical Earthquake Data (AHEAD) for the last 500 years. Error margins in magnitudes range between 0.3-0.5. Epicentral uncertainty of some of these earthquakes is very high such as the 1660, 1741, 1855, 1852, and 1887 earthquakes. It was noticed that higher-magnitude earthquakes (1741, 1609, 1851,

1863, 1756, 1513, 1481) mostly have occurred farther away from the lake. 1869 earthquake with magnitude 6.8, on the other hand, is a close and strong one. Another remarkable thing is that compared to the historical period, there are only a few examples of very strong earthquakes in instrumental periods (Figure 1.4). Onland and offshore active faults which might be related to the both instrumental and historical earthquakes in the region were also illustrated in Figure 1.4 (Emre Ö et al., 2011; Sakellariou & Tsampouraki-Kraounaki, 2018)

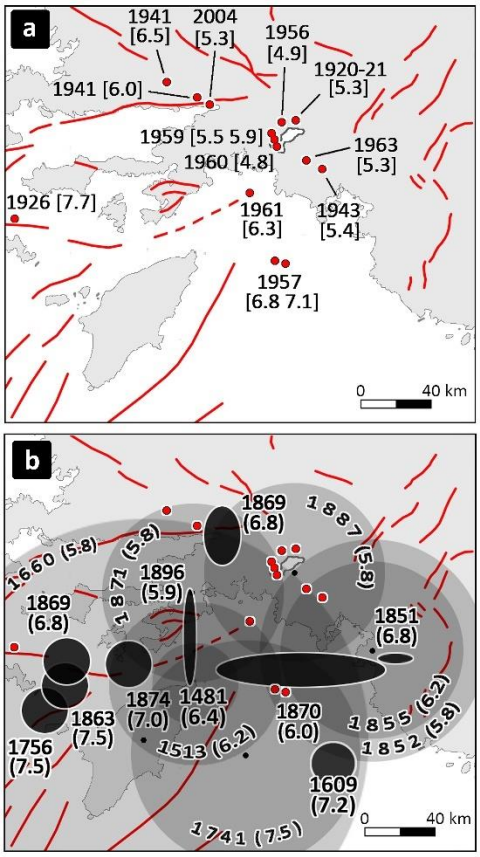

Year (CE)	Magnitude
1896	5.9 ± 0.3
1887	5.8 ± 0.5
1874	7.0 ± 0.5
1871	5.8 ± 0.5
1870	6.0 ± 0.3
1869	6.8 ± 0.4
1869	6.8 ± 0.3
1863	7.5 ± 0.3
1855	6.2 ± 0.5
1852	5.8 ± 0.5
1851	6.8 ± 0.3
1756	7.5 ± 0.3
1741	7.5 ± 0.3
1660	5.8 ± 0.5
1609	7.2 ± 0.5
1513	6.2 ± 0.4
1481	6.4 ± 0.3

Figure 1.4. Instrumental and historical earthquakes and faults around Köyceğiz lake. a) Instrumental earthquake years with given magnitudes (in brackets) and locations (red dots)(BDTİM, 2022). b) Historical earthquake years with estimated magnitudes (in bracket) and uncertainty of epicentral locations (grey and black circles and ellipses) (Albini et al., 2013). Errors in magnitudes of historically recorded earthquakes were given. Onland faults (adopted from active faults map of Emre et al., 2011) and offshore faults (adopted from Sakellariou & Tsampouraki-Kraounaki, 2018)

CHAPTER 2

MATERIALS AND METHODS

The main methods applied in this study include interpretation of bathymetric images for selecting suitable sediment coring sites, sediment coring using gravity corer for detailed analysis of sedimentary features, core-splitting and u-channel extraction to precisely scan the sediments by ITRAX-Micro XRF core scanner and radiographic imaging, ITRAX-Micro XRF core scanner, and radiographic imaging to reach and observe geochemical data, microstructures and possible soft sediment deformations of the core. The core chronology was obtained by varve counting (verified by ^{137}Cs and ^{210}Pb (Avşar et al., 2016)) to reach precise chronology to correlate them with historically and instrumentally known earthquakes and correlate cores with each other stratigraphically.

2.1 Bathymetric Survey and Sediment Coring

The bathymetric survey is basically the starting point for collecting information about the lake. It provides the bottom bathymetry of the lake basin. (Figure 1).

bathymetric images are very important for selecting suitable coring sites. For example; deep, flat, depocenter are preferred over slope areas where sediment bypass, channels with possible hiatuses might exist (Goldfinger 2011). For this purpose, bathymetric image of the Köyceğiz lake obtained from Avşar et al. (2016) is used. Locating the suitable coring sites was accomplished by careful analysis of this bathymetric image.

The selection of the coring technique is another important issue. Although, most of the coring methods are performed by penetrating the tube into the sediments

vertically, they use different riving forces and equipment. For example, while gravity corer consists of three main parts, (1) PVC liner, (2) brass weight, (3) valve flap, piston corer consists of six main parts, (1) core catcher, (2) piston, (3) PVC liner, (4) anvil, (5) doughnut hammer, and (6) guide rod. In addition, the driving force of gravity corer is the gravitational force that causes the penetration of the tube into sediments, in the piston corer technique, hammering provides force to penetrate the tube into sediments. While studying the laminated lake sediment, as in the Köyceğiz lake, the sediment-water interface must be undisturbed and complete (Avşar, 2013). In order to avoid any loss and deterioration of the sediment-water interface gravity coring technique was applied. However, still, there might be disturbance or loss in the water-sediment interface, so the top of the core was carefully examined immediately after it was taken. The coring procedure was repeated in the case if any mixing was observed in the water-sediment interface on top of the corer. The gravity corer principle is based on releasing the corer certain height from the water-sediment interface to free fall with the effect of gravity. While the tube is falling and penetrating, the valve flap that stands on top of the tube opens and allows water and sediment intake inside the PVC liner. After optimum penetration is achieved, the corer is retracted, and the valve flap is closed, which creates a vacuum that prevents sediment loss. It is important to mention that sediment recovery amount depends on free-fall height. If it is insufficient poor penetration may cause poor sediment recovery. If it is above a specific level, tilting may occur and cause non-vertical penetration and brass weight on the corer. This should be the maximum possible weight to minimize maximum free fall height. In this study, a 42 kg brass weight was used, and free fall height was set as 2-3 m from the bottom of the lake. Moreover, the valve flap characteristic is another criterion to avoid sediment loss at the sediment-water interface. It should be light and move freely. If not, it may cause turbulence ahead PVC liner and prevent water flow inside the liner. The 19 cores, a total of 23.66 m in length, were retrieved from Köyceğiz lake by gravity corer within the scope of this study. Six of them belong to the northern basin, and the other 13 are retrieved from the southern basin (Table 2.1)

Table 2.1. Coordinates and length of 19 cores

Core No	N	E	Length (cm)
1	4082372	643761	120.40
2	4082591	644321	126.50
3	4083196	644361	108.50
4	4082997	643631	120.70
5	4082608	643022	123.80
6	4083150	643056	117.55
7	4083612	643689	122.50
8	4083900	644176	127.10
9	4083670	643168	132.40
10	4084164	643582	132.00
11	4083598	642484	118.80
12	4084101	642972	98.80
13	4084563	642921	132.20
14	4089391	649204	132.20
15	4089062	649866	120.50
16	4089611	650102	133.46
17	4090186	649972	127.60
18	4089812	649552	132.70
19	4090201	649102	138.70

2.2 Core Splitting and U-Channel Extraction

The first step of this method is cutting the core in half. The procedure is to put cores and fix them with plastic clumps to avoid damaging the cutting platform, including cutting discs. Later, splitting the cores into halves to use one half in the u-channel extraction process. The other halves were kept in the cold room at the temperature of their natural environment to prevent any cracking and shrinkage related to loss of water for the necessities of using these second halves.

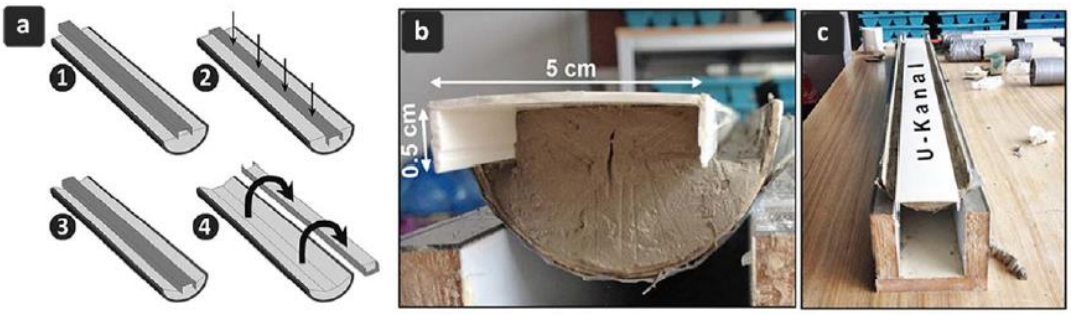

Figure 2.1. U-channel extraction process. a) Steps represents u-channel extraction processes. b) Cross-sectional view of processes and dimensions of plastic cable channel. c) Top-view of the processes.

The second step is the u-channel extraction process, which is made by using plastic cable channels that are mainly used for collecting and hiding the cables. These plastic cable channels were pressed in the chosen mid-line carefully and slowly, then the channel was split from the core beginning through the end with fishing line apparatus, and its surface was flattened and covered with stretch film (Figure 2.1). This procedure was applied to 19 cores to increase the reliability and clarity of the data collected from the ITRAX scanning and radiographic imaging (Avşar et al., 2016). The final stage is sending these extracted u-channels to the ITRAX scanning and radiographic imaging.

2.3 ITRAX Micro-XRF Core Scanning

This non-destructive and high-resolution method provides useful geochemical data from terrestrial, lacustrine, marine sediments, and drilled rock cores. ITRAX Micro-XRF Core Scanning is one of the most common methods that can be applied to examine paleoenvironmental and sedimentological processes (Croudace & Rothwell, 2015). ITRAX Micro-XRF Core Scanning is preferable since it can produce optical, radiographic images and elemental variations (Croudace et al., 2006) directly from half cores and/or u-channeled sediments. Radiographic images can be provided due to x-radiograph incorporation, ideally suited to the analysis of varved sequences, increasing the interest of this scanner usage in lacustrine research.

In addition to that, this scanner allows for the rapid and non-destructive recording of element proxy variations at decadal, annual, and even sub-annual timescales (Croudace & Rothwell, 2015). X-ray tube decision before the scanning should be done with respect to elements that are crucial to be detected due to the aim of the study. Molybdenum (Mo) and chromium (Cr) are the most common X-ray tubes of ITRAX devices. Mo X-ray tubes detect transition and heavy elements in better resolution, while the Cr X-ray tube is optimal for lighter elements (e.g., K, Ca, Ti) (Croudace et al., 2006; Rothwell et al., 2006). Other important parameters that should be set before scanning are dwell time and measurement increment. The standard procedure of this method starts with positioning the half-core and/or u-channeled sediments on the horizontal cradle. The second step is the scanning to obtain the topography of the half core, but this step can be skipped for the u-channel sediments since the surface of the sediments has already been straightened during extraction. The third step is choosing the range of expected elements and setting peak fitting parameters, then setting dwelling time to spend on each point of the u-channel sediments and measurement increments to serve the purpose of required resolution (e.g., 200 µm for laminae) (Croudace et al., 2006; Rothwell et al., 2006).

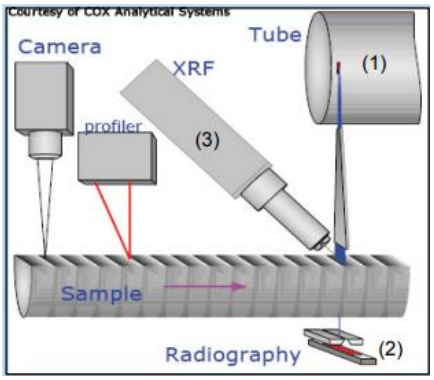

Figure 2.2. ITRAX Micro XRF system (Croudace et al., 2006). (1) X-ray tube, (2) radiography, (3) XRF.

The Working principle of ITRAX (Figure 2.2) is to send an X-ray beam to each measurement point on the core and plot the incident energy graph of the X-ray versus the sample's photon emission intensity. Each element emits a photon with different X-ray energy levels, and emission rates (e.g., peak height) highly depend on the

number of elements within the scanning sample. Detection and area calculation of these peaks are done automatically by the software used by ITRAX. Elemental variations of scanned core might be misinterpreted if elemental data from ITRAX is examined directly because some sediment properties (e.g., porosity, organic matter, and water content) have negative effects on measurement precision (Croudace et al., 2006; Löwemark et al., 2011; Thomson et al., 2006). In order to achieve more precise and reliable results related to paleoenvironmental and paleoclimatic conditions, inter-element ratios should be analyzed (e.g., Croudace et al., 2006; Rothwell, 2006; Thomson et al., 2006; Avşar, 2013). The results are not quantitative but semi-quantitative means that it gives the elemental concentration data that can be used to make the comparison in between. However, data should be standardized before comparing different elements with a very simple formula.

$$z=(x-\mu)/\sigma$$

Where z is the standardized value, x is the data value, μ is the mean value, and σ is the standard deviation of the data set. This standardized value will be ready for comparing the data properly (Croudace et al., 2006; Rothwell et al., 2006; Avşar, 2013). Additionally, the radiographic image provides information related to the bulk density of sediments, when the image is darker, it implies higher density which might indicate terrestrial influx, when color is lighter, it might indicate subaqueous deposition.

The Marine Research Department of the General Directorate of Mineral Research and Exploration (MTA), ITRAX laboratory, was used as a sediment core scanning procedure in this study. Measurement increments were set as 1 mm resolution except for core numbers 6 (0.5 mm), 9 (0.2 mm), and 16 (0.2 mm) for Köyceğiz varve sediments, and dwell time was set as 5 seconds except for core number 9 and 16 (7 seconds). The tube was selected as Mo type concerning the aim of this research.

2.4 Core Chronology

There is various technique to date lacustrine sedimentary sequences, such as radiocarbon and short-life radionuclide dating, varve counting, paleomagnetism, and tephrochronology. It is important to apply a suitable technique that basically depends on the sediment or rock type and the objective of the study. Due to the great importance of stratigraphic and chronologic correlation, the core should be dated very precisely and accurately, as mentioned previously. Within the scope of this study, the core chronology was obtained by varve counting and radionuclide dating. Radionuclide dating was applied to avoid confusion related to laminae, whether they are deposited annually (seasonally) or not (Avşar et al., 2016). Since ^{137}Cs and ^{210}Pb date recent sediments, these radionucleide dating methods also provide calibration points during varve counting. Applied radionuclide dating methods were ^{137}Cs and ^{210}Pb. Under stable environment conditions with uniform sedimentation, the ^{210}Pb method is very reliable, but it can provide good results even for non-uniform sedimentation (Appleby, 2005). To control the reliability of the ^{210}Pb method, ^{137}Cs (artificial radionuclide having 30 years half-life) can be used because there were nuclear weapon tests between 1954-1963 and the 1986 Chernobyl explosion. The sudden rising in the amount of artificial cesium isotope can indicate the exact time of the studied sediment layer. In Avşar et al. (2016), laminations of Köyceğiz lake were claimed to be deposited annually based on the results of ^{137}Cs and ^{210}Pb age dating methods.

Subsequently,, these annually deposited carbonaceous laminae of core number 13 were counted since it provides relatively longer sediment stratigraphy and clearer appearance of laminae by using optical images of varve sequences provided by the ITRAX micro-XRF core scanner. In some levels, carbonaceous laminae were hard to distinguish at that point sedimentation rate of neighboring levels, and lateral continuity of the laminae were taken into account during counting. The counting process was applied until reaching uncertain regular varve formation levels. These levels were not considered as varve deposits.

2.5 Core-to-core Correlation

Identification of the source and triggering mechanism of event deposits is crucial as mentioned before, spatial distribution of these event deposits is important in this sense. Additionally, investigating the spatial extent of event deposits can be useful in detecting intensity of events, such as intensities of paleoearthquakes can be determined by cumulative turbidite thickness (Moernaut et al., 2014). Observing the spatial distribution of event deposits and having complete event stratigraphy core-to-core correlation is vital. Also, core-to-core correlation is very critical since it is hard to obtain thin deposits such as tephras and thin turbidites' spatial distribution by tracing subbottom profiles. In order to correlate the cores, there exist many methods and strategies. One of them is related to following color alteration within laminated sediments of cores taken and correlating them with each other, which can provide mm-scale accuracy. The other one is, correlating the abrupt or gradual change in background sedimentation that can be observed by continuous scanning and logging data with XRF, CT, magnetic susceptibility, and so on. Another one is when background sedimentation is homogeneous, and it is hard to provide a high-resolution temporal correlation. Still, if there exists a marker bed such as tephra which is very useful for age dating, it can be used to correlate cores by tracking it. Moreover, varve counting is very practical while producing the core chronology, and thanks to color contrast between annually deposited laminae, it can also be useful while correlating cores.

Within the scope of this study core to core correlations were done by correlating core number 13 with other eighteen cores via ITRAX-produced elemental data and optical images. Peaks of subaquatic versus terrestrial element ratios (e.g., Ca/Ti, Cr/Ti) of cores were compared, and the depth of these peaks' was checked in optical images to be on the safe side while correlating cores. Afterward, cores were correlated one by one with the 13th core with respect to matching peak points of elemental ratios. However, some peaks are hard to distinguish; therefore, optical images of cores were compared, and distinct layers were tried to be correlated. Late, the chosen peak points

(approximately 12 points) and their respective depths were used in MATLAB 2020a software to create matching points of cores throughout their length. These values are then carefully checked by controlling the correlated graphs of cores. If controlled graphs were well-fitted, they were left as they were, but if they were not, the processes were repeated until they fit well.

2.6 Calculation of the Deformation Index

The deformation index was determined in three stages. First, laminae were drawn as lines in photoshop. Intraclast breccias and upper terminations of faults were drawn as zigzag lines. Second, these drawings were georeferenced in ArcGIS. The raster images of lines along each core were binarized by the resampling method in ArcGIS. Then, the binary images were converted into polylines. Afterward, the polylines were transformed into equally distant points (1 mm distance). The X and Y coordinates of these points were extracted. Finally, linear regression was applied to each line and best fit line was generated, and mean square error (MSE) was excepted as the deformation index (DI) for each line. MSE was automize through MATLAB script (Avşar et al., 2016) to enable fast and practical output of DI.

2.7 Peak Ground Acceleration (PGA) and Peak Ground Displacement (PGD)

For PGA Avşar et al. (2016) was adopted calculation. In addition, Crowell et al. (2013) attenuation relationship was used to calculate PGD. The PGD plot was obtained by considering the uncertainty of historical earthquakes parameters (epicentral distance, magnitude).

CHAPTER 3

RESULTS

According to optical images of 19 cores retrieved from Köyceğiz lake, 3 types of SSDS were observed, and distinct ones are illustrated. These SSDS are i) faults (Figure 3.1, Figure 3.2), ii) intraclast breccias (IB) (Figure 3.3), and iii) disturbed laminations (DL) (Figure 3.4). Observation of upper termination inside the cores provides an opportunity to evaluate their chronological relationship with past earthquakes. Otherwise, any interpretation related to the timing of faulting will be speculation if the information related to whether faults are sealed by a younger undisturbed sedimentary level (or not) at the upper parts of the cores. Juxtaposed laminae along the fault indicate vertical movement of the fault blocks. Most faults observed in Köyceğiz cores show normal sense of motion. Amount of offset decrease gradually towards the upper termination. The offset amount is approximately reaching up to 8 mm (e.g., Figure 3.1g). It is important to note that the faults are rarely observed at the upper levels of the cores (e.g., Figure 3.1a, Figure 3.2c). On some occasions, minor antithetic faults were detected along with the master fault (Figure 3.1c). It has been recognized that intraclast breccias overlay some observable upper terminations of faults (Figure 3.1b,d,g,f, Figure 3.2e,d), and some faults traverse brecciated layers (Figure 3.1b,d,f- Figure 3.2a,d,e,h). Most of the faults display listric geometry.

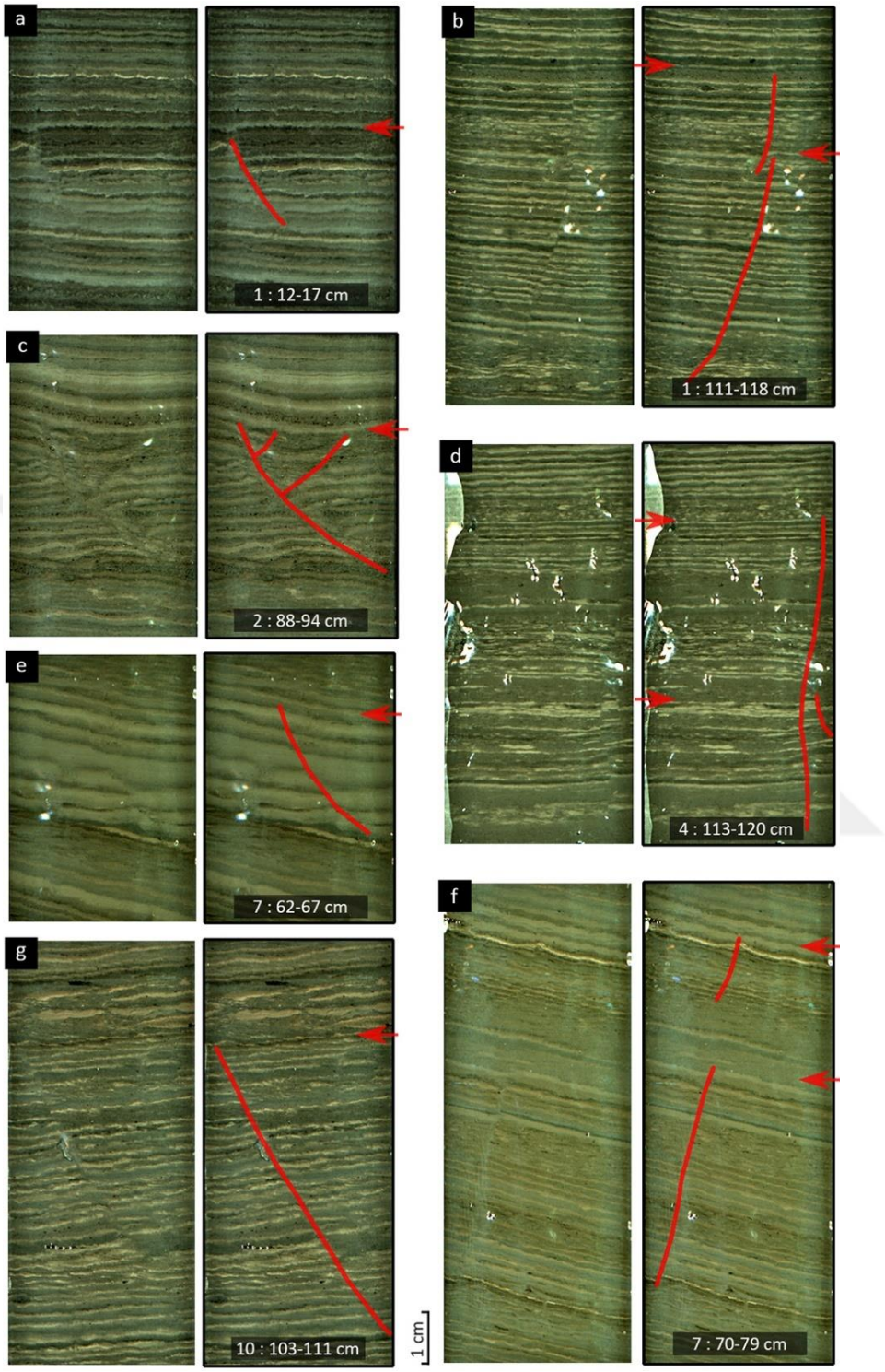

Figure 3.1. 7 Distinct faults (a-g) observed in optical images of the cores in cm scale. Core numbers and depth of core sections were shown at the bottom corner of the core images. Red arrows indicate the upper termination of the faults.

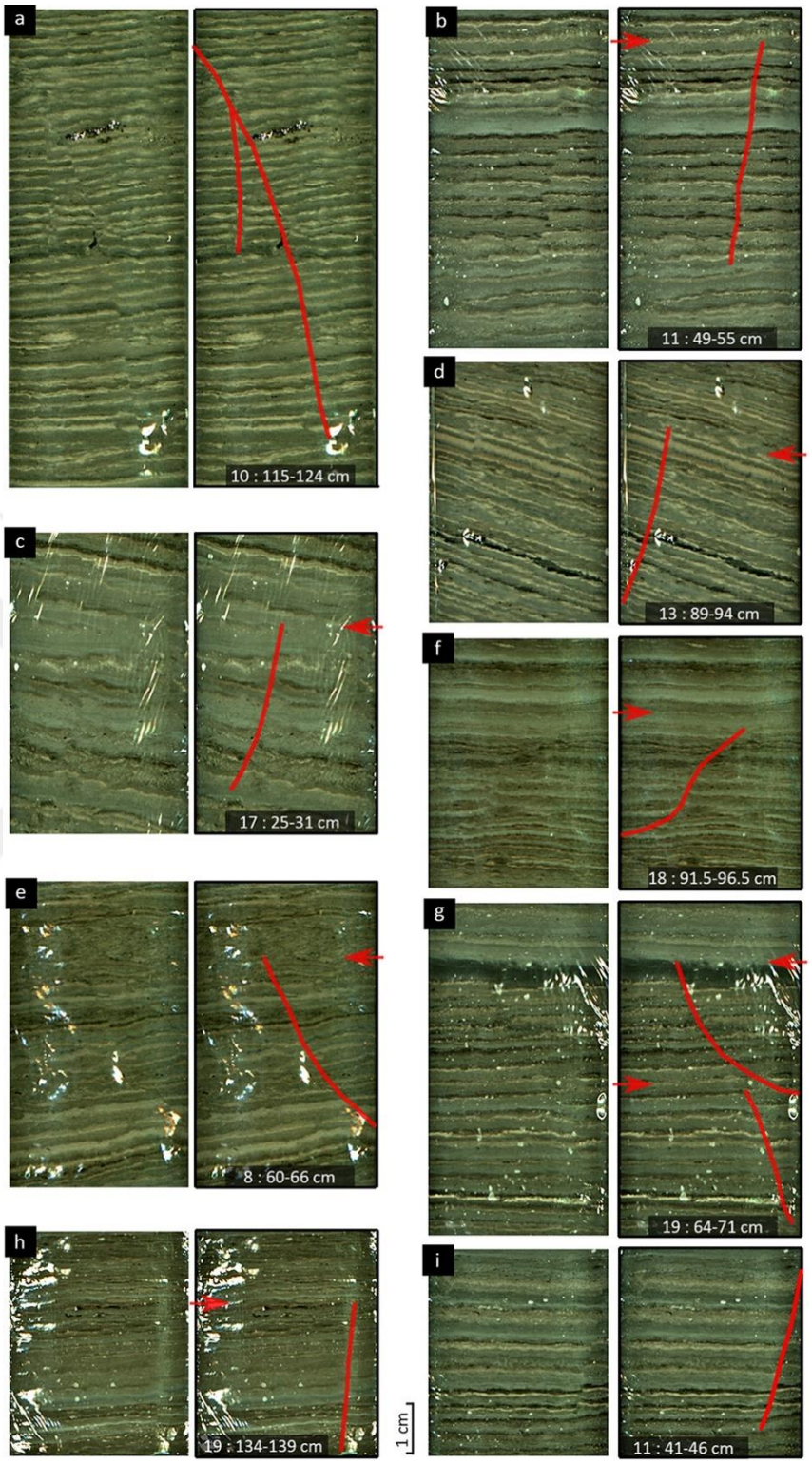

Figure 3.2. 9 Distinct faults (a-i) observed in optical images of the cores in cm scale. Core numbers and depth of core sections were shown at the bottom corner of the core images. Red arrows indicate the upper termination of the faults.

The breccias observed in the core pictures show striking differences at first glance. These differences are primarily related to the presence of observable carbonaceous brecciated laminae fragments within the undisturbed laminae boundaries (Figure 3.3a,b). In some cases, these brecciated carbonaceous laminae are become completely unobservable (Figure 3.3b). Another prominent difference is related to the number of brecciated laminae that are enveloped by two intact layers. Stratigraphic levels where 3 or more laminae brecciated are considered distinct intraclast breccias (Figure 3.3c). It has been recognized that the frequency of intraclast breccias increases towards to bottom of the cores. In addition, IB was not observed at any upper levels of the cores. When the cores were examined by considering the sedimentation rate, it was recognized that distinctly thick laminae had not been brecciated.

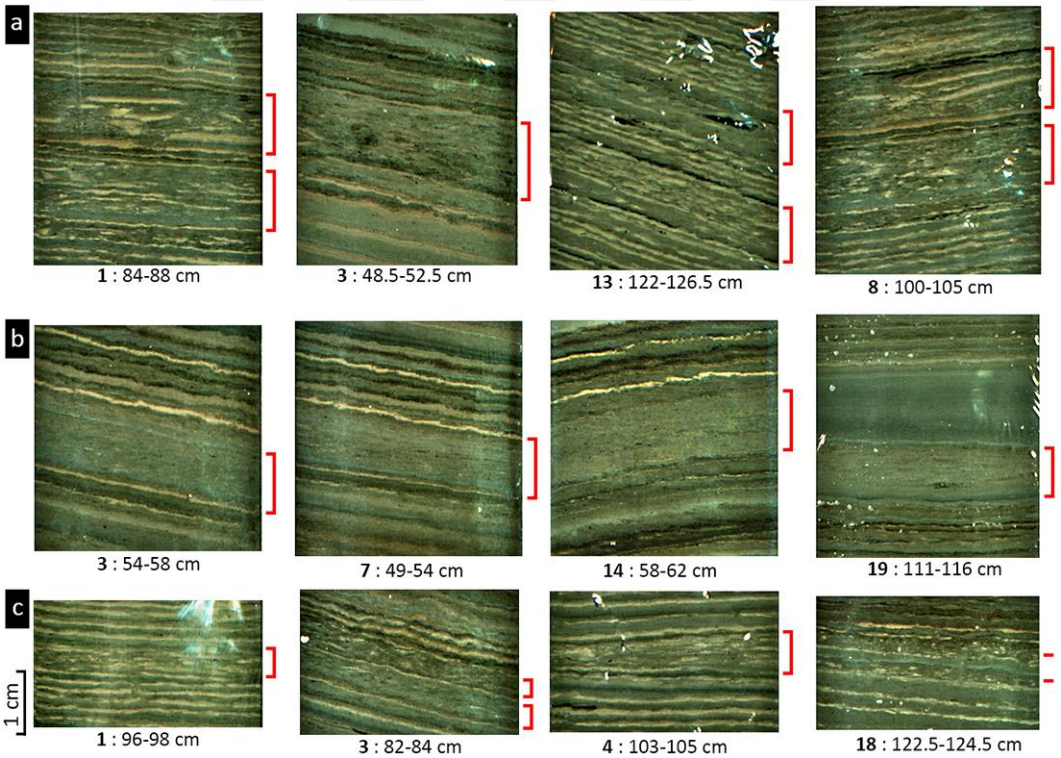

Figure 3.3. Intraclast breccias observed in optical images of the cores in cm scale. Boundaries of IB were shown with red brackets, and core numbers and depth values were shown below each core section.

In core images, some carbonaceous layers lose their original form and display undulations (disturbed lamination). These undulations are visually distinct (Figure 3.4a) or vague (Figure 3.4b) in certain levels of the cores. Moreover, some layers show tilting in between the horizontally straight laminae (e.g., Figure 3.4b core number 1). Therefore, other inclination that was observed in optical images are related to slight tilting of corer during penetration.

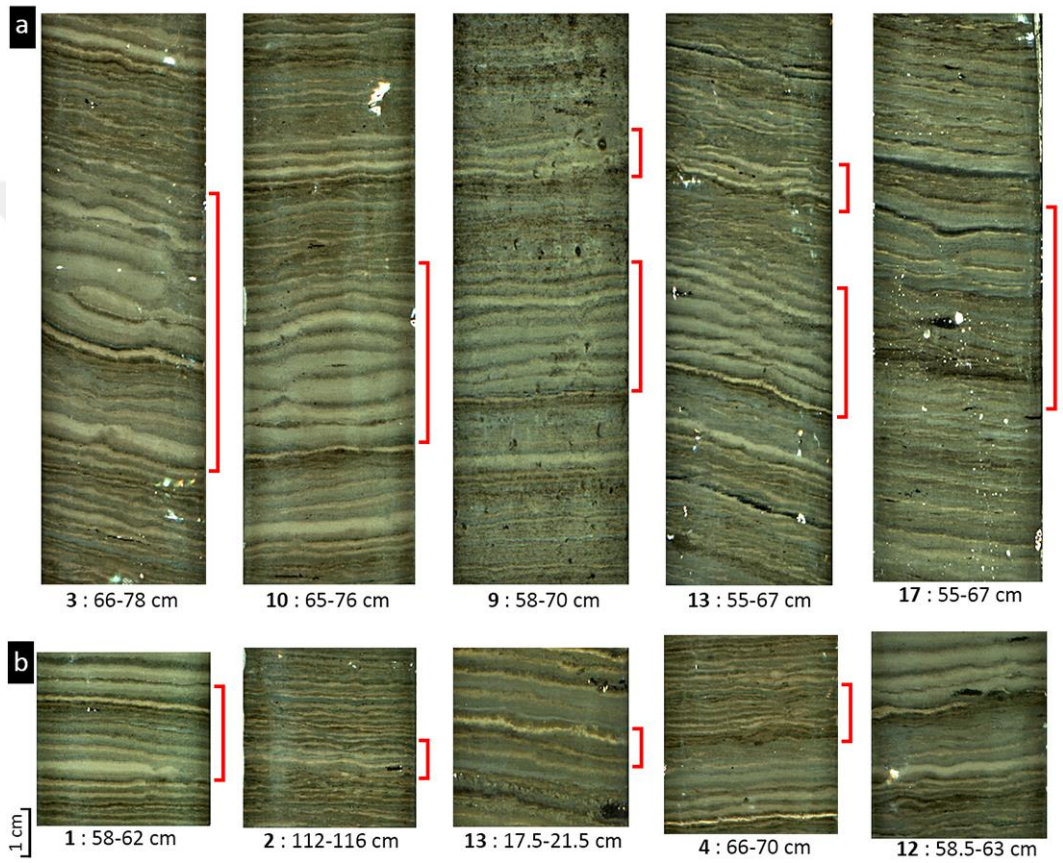

Figure 3.4. Disturbed laminations observed in optical images of the cores in cm scale. a) visually distinct DL showed by red bracket. b) vague DL showed by red bracket. Core numbers and depth of core sections were given below each image.

In addition to SSDS, there exist some levels with a lack of carbonaceous laminae. It has been observed that some of these sections are relatively thicker than others (Figure 3.5 top row), and some of them are repetitive (Figure 3.5 three cores in the lower right corner). Except for core number 4, all these levels belong to the cores that were retrieved from the northern basin. A possible explanation of the extinction

of the carbonaceous laminae might be mainly related to change in climatic conditions (e.g., floods, change in water chemistry) or instantaneous event deposition (e.g., seismoturbidites, slumps), which will be discussed in the next chapter. These instantaneous deposits were removed from the sequence to obtain varve counting-based chronology.

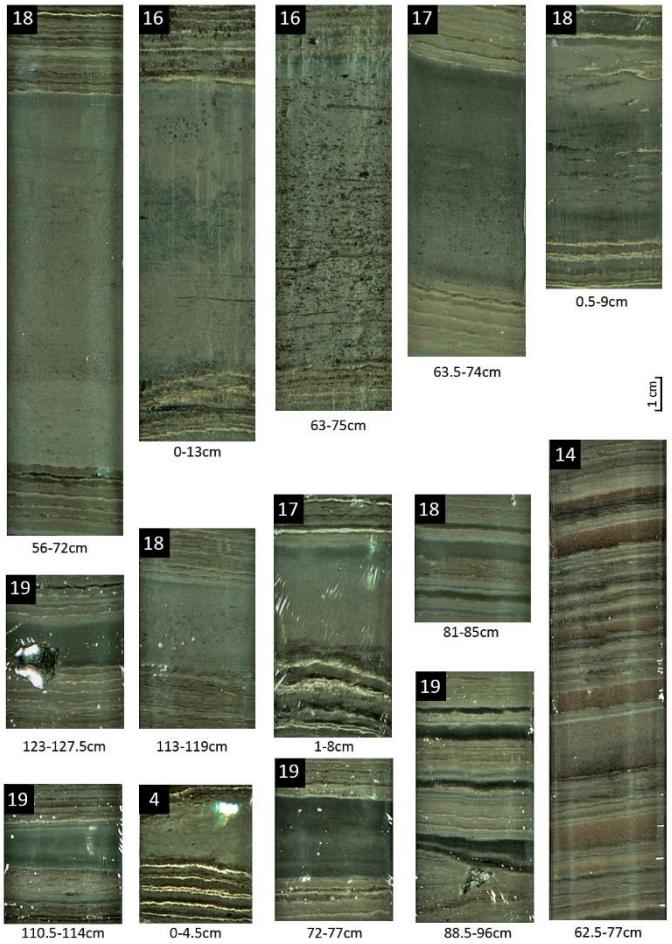

Figure 3.5. Absence of carbonaceous laminae in core intervals. Core numbers (top left corner) and depth values (below each core) were given in cm scale.

The core chronology of core number 13 was obtained by varve counting, and a total of 578 varves was determined (Figure 3.6 & Figure 3.7). Since cores were retrieved in 2017, the age of the varve with a depth of 130.5 cm is calculated as 1440. The uncertainty related to regular varve formation observed at the bottom of the core was decided to be excluded from the counting process (Figure 3.7). The average

sedimentation rate that was acquired from the age-depth model is yielded as 0.23 cm/yr, which is consistent with the sedimentation rate calculated by Karadaş (2022).

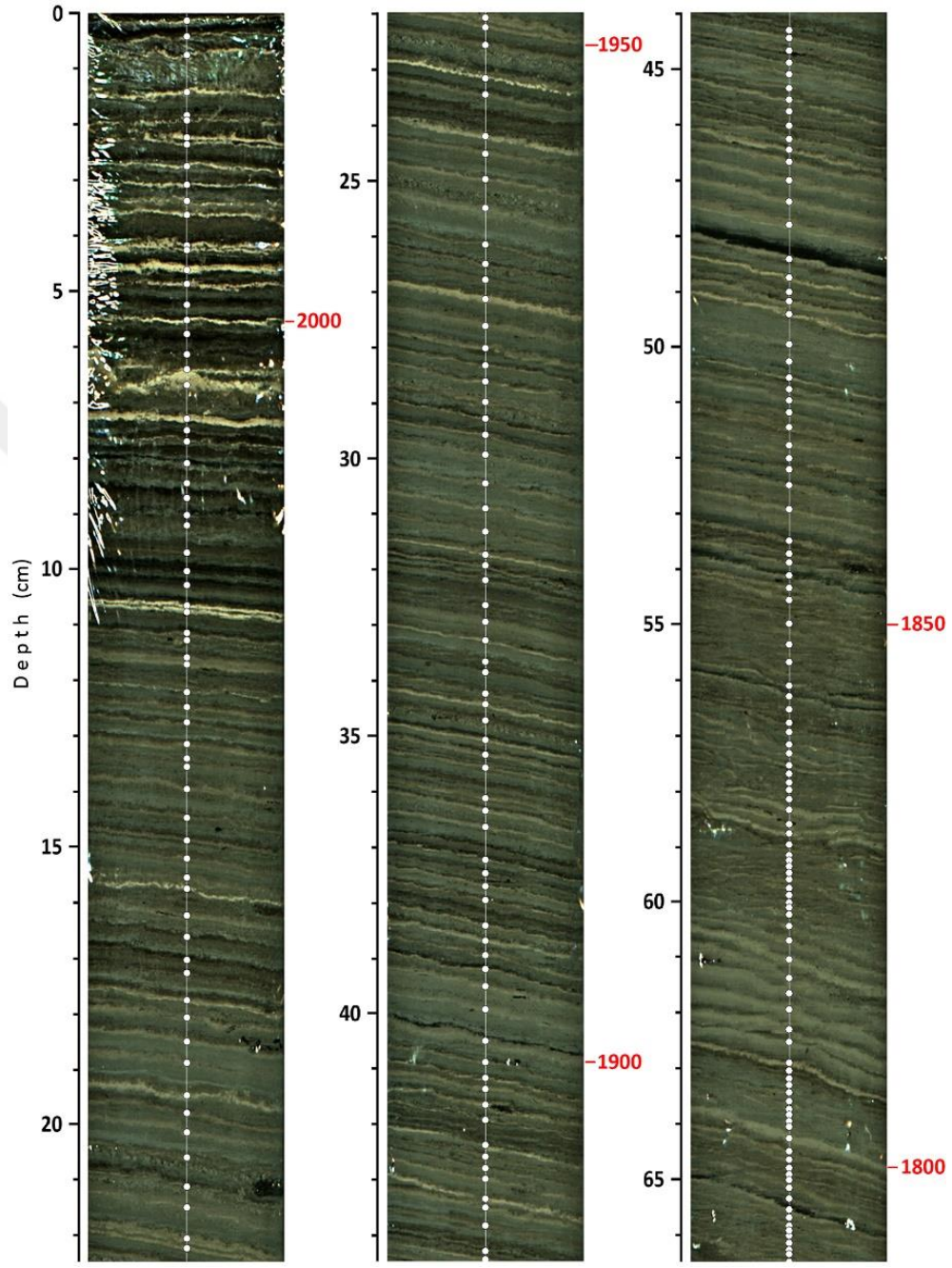

Figure 3.6. Varve counting of core number 13. White dots indicate counted carbonaceous laminae, and the ages of laminae on 50 years scale were shown on the right side of the core with a given depth in cm

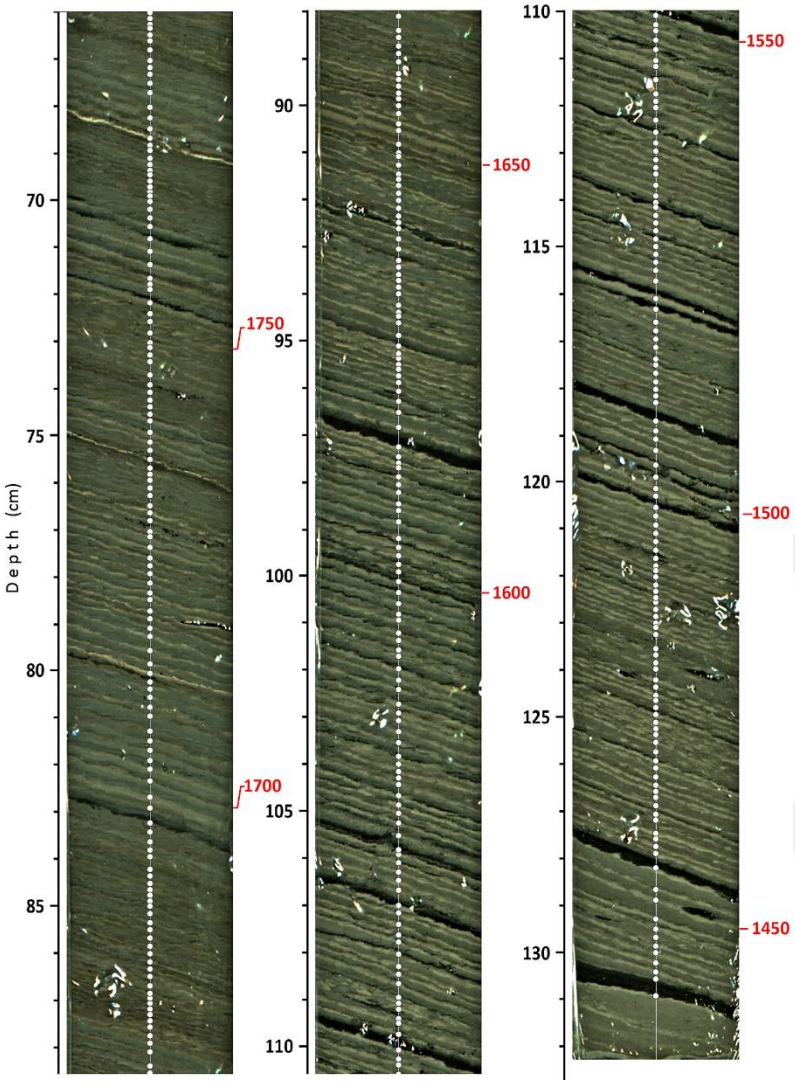

Figure 3.7. Varve counting of core number 13. White dots indicate counted carbonaceous laminae, and the ages of laminae on 50 years scale were shown on the right side of the core with a given depth in cm.

While examining optical images of 19 cores, it was noticed that visual marker layers are well-correlated with each other (Figure 3.8). Thus, 7 distinct marker laminae of each core with different depth values provided an opportunity to correlate cores based on these compatible marker layers. Two cores (6 and 16) with low resolution due to sliding or uncovering with plastic foil did not allow to distinguish any deformation in the related depths, so these parts of the cores were excluded from the SSDS illustration process (Figure 3.8). In a few cores, regular varve formation was not observed towards their bottom (e.g., Figure 3.8 cores 14,18). It was recognized

that in some levels slope of correlation lines is significantly different than the slope of one below (e.g, Figure 3.8 correlation lines 2, 1 between cores 17, 19, and 18, 19). The possible main explanations for this observation might be a change in sedimentation rate, sudden increase in overburden pressure due to instantaneous deposits, faulting (omission or repetition of strata), and change in slope of laminae due to core tilting or deformation.

Instantaneous deposits are the most common in the northern basin. It was observed that the most recent instantaneous deposits of cores belonging to the northern basin are well-correlated with each other (Figure 3.8, topmost part of cores 14,15,16,17,18,19). Instantaneous deposits that were observed in the middle part of the cores do not temporally correlate as in the case of the most recent one. Three different instantaneous deposits were observed at this level; the oldest ones, observed in core number 14, are repetitive. The other one is correlatable between core numbers 17, 18, and 19. Between these two instantaneous deposits, another one that correlates among 15, 16, and 17. Some independent instantaneous deposits were observed at the lower part of these northern basin cores.

The major distinct SSDS (IB, DL, and faults) were represented by different colors (green, blue and red, respectively) in this correlation figure to observe their relation at first sight. It was noticed that SSDS are more common in the southern basin and below the correlation line 3 at first glance. Notably, these three types of deformations are successive in a few levels (e.g, Figure 3.8 core 2 below the 7th line, core 19 below the 7th line). IB seems to be the most common SSDS type, especially through the bottom of the cores. Based on visual inspection, IB in 1869 are well-correlated throughout all cores. On the other hand, IB in 1754 are correlatable among southern basin cores. Most faults with observable upper termination are not correlatable based on visual inspection. Most of the visually distinct LDs also seem incompatible, but between correlation lines 4 and 5 among cores 2, 3, 10, and 8, the thickest carbonaceous laminae disturbance is well-correlated. Besides these distinct SSDS, minor deformations will be shown by the deformation index in the discussion chapter. In this correlation figure, another striking recognition is that the upper part of the cores lack of deformation.

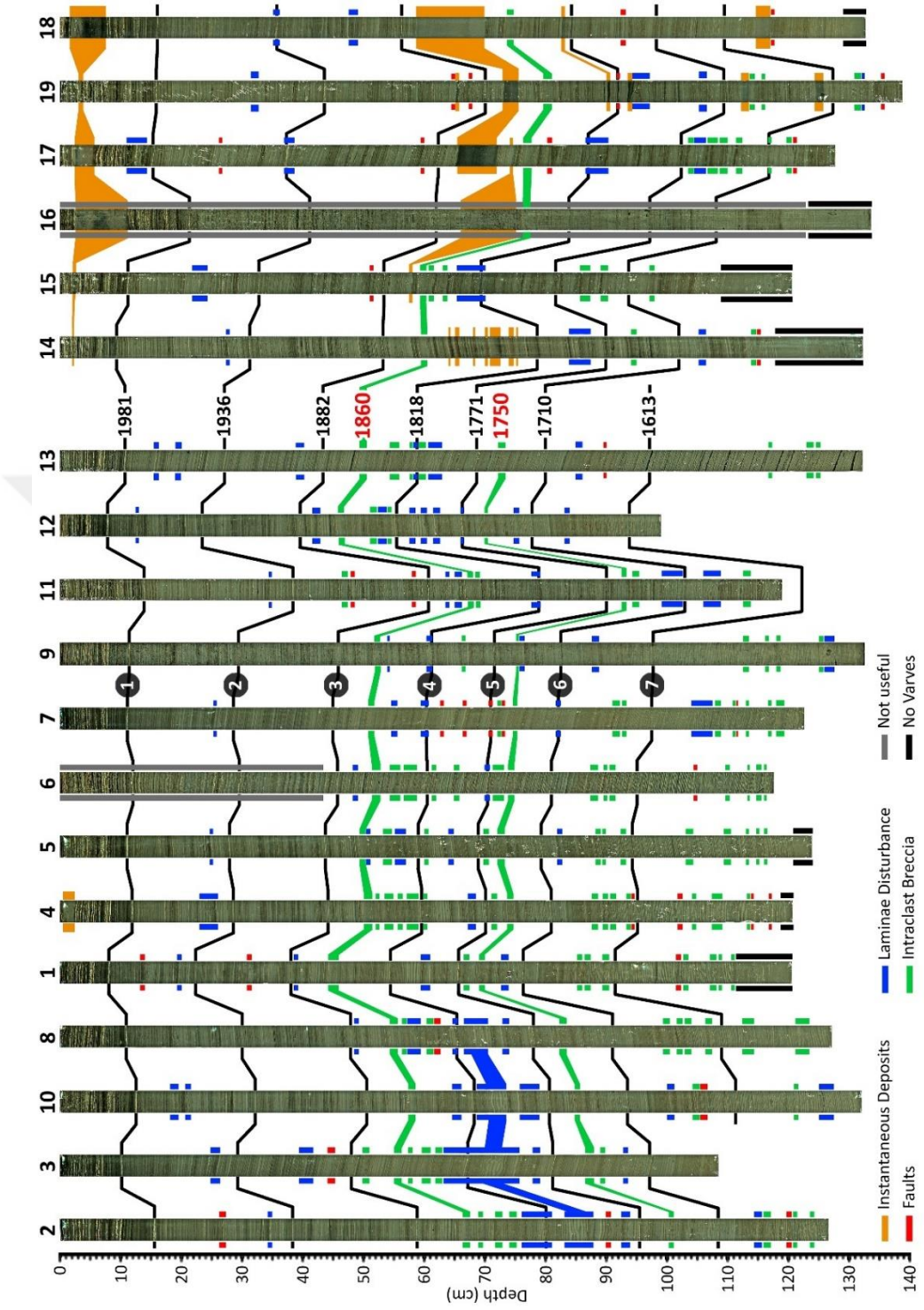

Figure 3.8. Correlation of optical images from 19 cores (related core numbers were given above each core) shown by 7 horizontal black line with years based on varve counting. Coeval SSDS and instantaneous deposits were correlated with respect to their assigned color as shown in the legend.

Illustration of these different modes of deformations based on 7 distinct marker layers, on correlation figure, provided opportunity to compare 19 cores in more detail. A close-up view of these 7 marker layers was prepared to show their compatibility (Figure 3.9). Moreover, Ca/Ti peaks observed in the related depth of these 7 marker laminae were correlated to support this compatibility. It was realized that geochemical data is highly correlatable as well. Eventhough, core to core correlations via compatible laminae seemed consistent outwardly; it will remain incapable of detailed evaluation of SSDS.

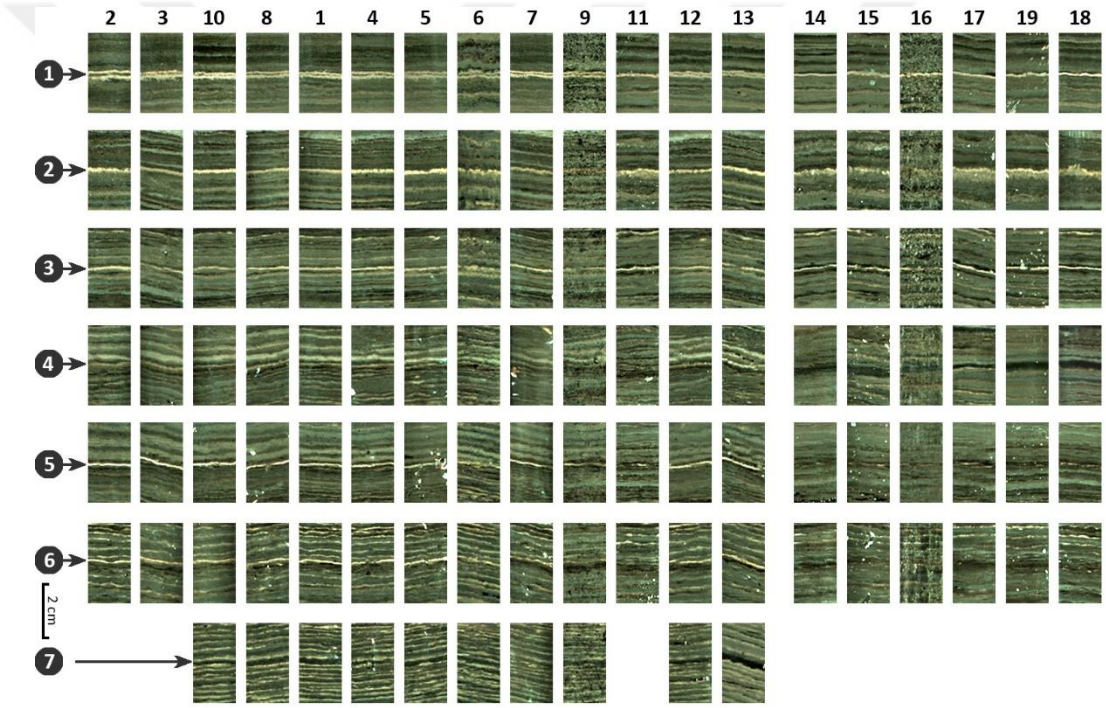

Figure 3.9. Close-up view of compatibility of 7 visually distinct marker laminae levels of 19 cores. Core numbers were shown top of each core. 7 marker laminae indicated by arrows.

The cores were correlated based on Ca/Ti and $(Cr,Ni)_{av}/(Ti,K,Fe)_{av}$ peaks of the 7 laminae observed in each core (Figure 3.10 and Figure 3.11). Ca/Ti is one of the most common paleoenvironmental proxies, so it was used while correlating cores. Compatibility of peaks of this ratio is more evident in some levels (e.g., Figure 3.10

1984, 1776) throughout the Köyceğiz cores. The correlation line that indicates 1890, on the other hand, shows consistency among the northern basin cores (14, 15, 16, 17, 18, and 19). Significant depressions recognized in cores 16, 17, 18, and 19 below 1890 are consistent with instantaneous deposits observed in the correlation figure. Chronological differences between these deposits became apparent when peaks were investigated in more detail. Thickness of these depressions and instantaneous deposits shown in the optical image also seems very relatable (Figure 3.10 below 1890 and above 1984 in cores belonging to the northern basin).

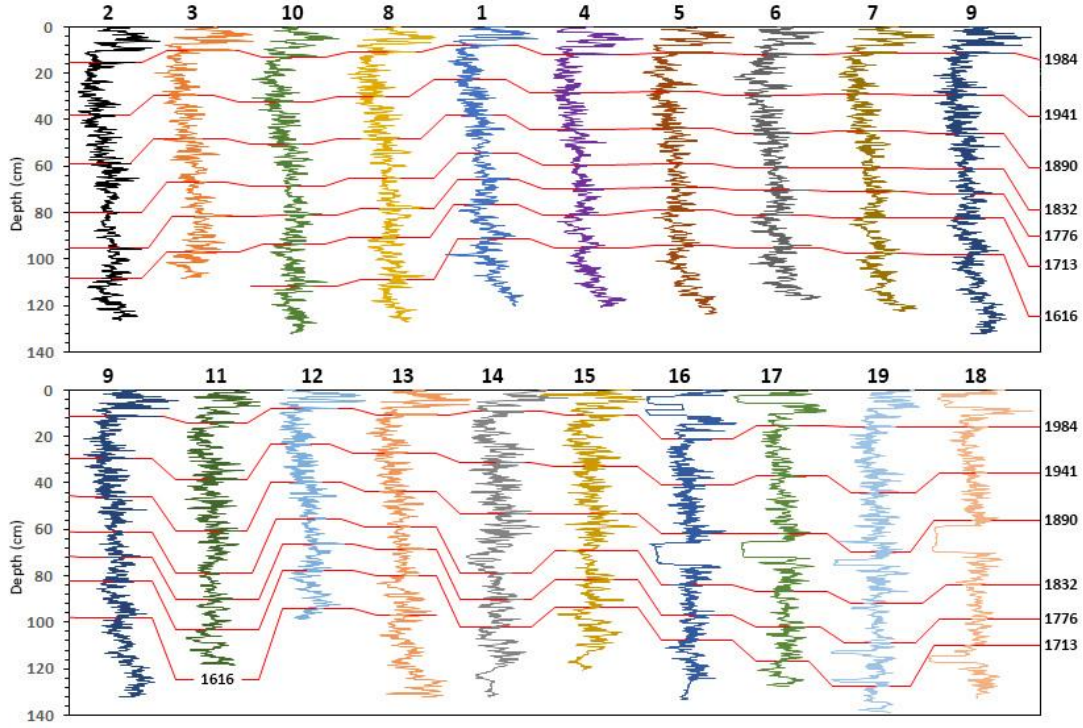

Figure 3.10. Correlation of Ca/Ti of 19 cores based on peaks of 7 marker laminae

Ratios of elements (Cr, Ni, Ti, Fe, and K) that were provided by ITRAX micro-XRF core scanner were examined to investigate change in source and composition of incoming detrital sediments to the lake. $(Cr,Ni)_{av}/(Ti,K,Fe)_{av}$ is a reliable paleoseismic proxy in mafic and ultramafic rocks dominated catchments since Cr and Ni (chemical weathering products of these rock types) enrichment is expected due to the seismic shock of earthquakes related increase in erosion rate (Avşar et al., 2016; Avşar et al., 2014). This ratio shows anomalies in all Köyceğiz lake cores

(Figure 3.11 between 1984 and 1941). Other significant amplified levels were observed in cores that belong to the northern basin, which is fed by three runoffs, and core number 11, which is close to the Sultaniye stream, around the first half of the 1800s (Figure 3.11).

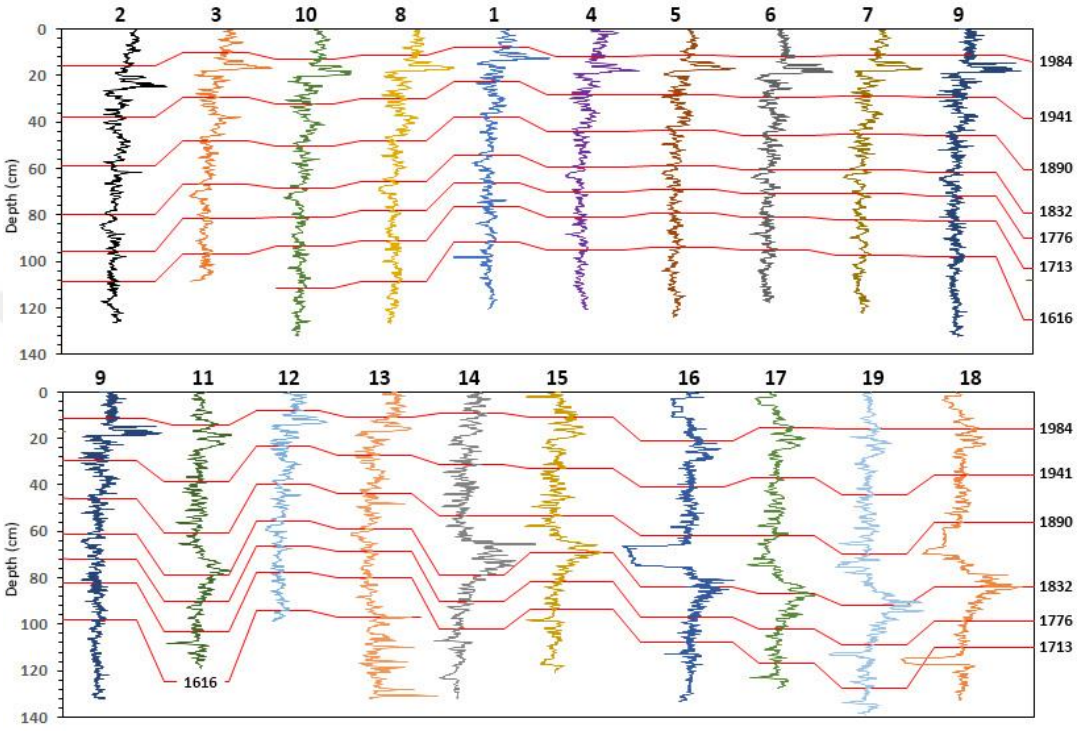

Figure 3.11. Correlation of $(Cr, Ni)_{av}/(Ti, K, Fe)_{av}$ of 19 cores based on 7 marker laminae with respect to depth.

CHAPTER 4

DISCUSSION

The importance of precise age dating and multi-coring becomes more obvious after precise correlation of cores was obtained. Köyceğiz cores can be visually correlated up to a certain point. Therefore, high-resolution ITRAX data was used for basin-wide correlation of seismites to evaluate SSDS better. Cores were correlated with core 13 one by one, corresponding to their Ca/Ti peaks (Figure 4.1 a). Geochemical signals of correlated cores show perfect harmony when overlapped (Figure 4.1 b). Close-up views of the correlated cores confirm this (Figure 4.1 c). The overall correlation of 19 cores shows strong consistency (Figure 4.2). Since varve-based chronology was obtained for core 13 and cores were correlated with this core, Ca/Ti graphs were given with years (Figure 4.2). Instantaneous deposits recognized in core 4 and cores from the northern (14,15,16,17,18,19) are excluded from the correlation process.

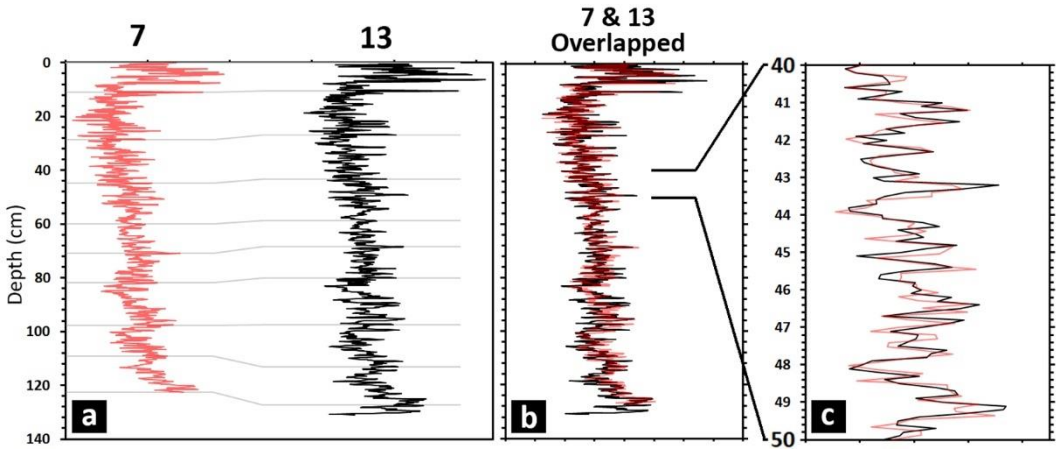

Figure 4.1. Correlation of core numbers 7 and 13 based on Ca/Ti with respect to depth a) Correlation of compatible peak points shown by grey lines. b) Overlapped view of 7 and 13 after correlation. c) Close-up view of correlated cores between the 40-50 cm.

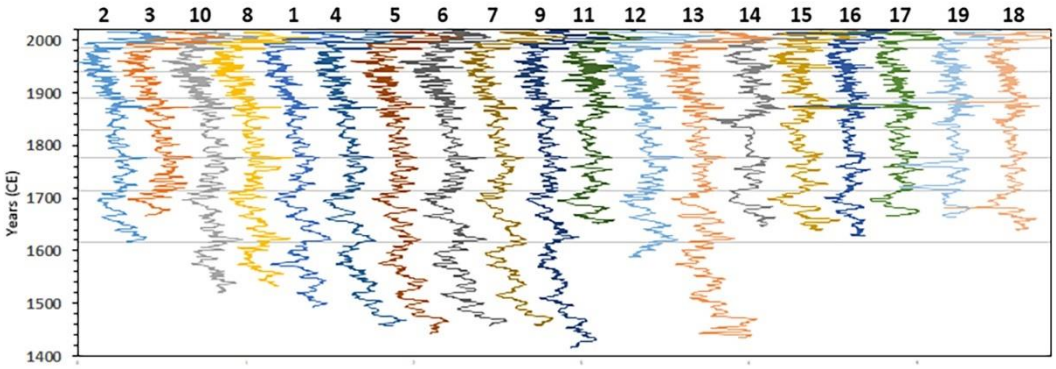

Figure 4.2. Correlation of Ca/Ti profile of 19 cores with respect to time.

4.1 Seismites

4.1.1 Catchment Response (CR)

$(Cr, Ni)_{av}/(Ti, K, Fe)_{av}$ ratio is claimed as a good paleoseismic proxy for lakes with mafic/ultramafic catchment lithology since weathering products of these rock types are enriched in Cr and Ni (Avşar et al., 2016). However, when comparing it with Cr/Ti ratio, the peaks were very consistent, but Cr/Ti ratio peaks are more noticeable. Therefore, Cr/Ti ratio is used to investigate CR-related anamolies instead of the $(Cr, Ni)_{av}/(Ti, K, Fe)_{av}$ ratio. The core locations and streams are shown in 53 to reveal the differences in catchment response (CR) signals observed in Cr/Ti graphs. It is observed that there are two levels (between 1980-1959 and 1850-1870) where Cr/Ti values have significant peaks. Avşar et al. (2016) assigned PGA threshold values as 70 $cm/s^{2,}$ which indicates these earthquakes have created at least 70 cm/s^2 PGA. The sudden increase of Cr/Ti in 1959 is observable in all cores; 1850 peak, on the other hand, is noticeable only in the northern basins cores and core 11. This discrepancy is related to stronger ground shaking of earthquakes between 1959-1980 than earthquakes that occurred in 2 decades after 1850. In addition, the northern basin is fed by a larger catchment than the southern basin. The CR signals observed in core 11 is most likely related to its proximity to recharge channel compared to other cores in the southern basin.

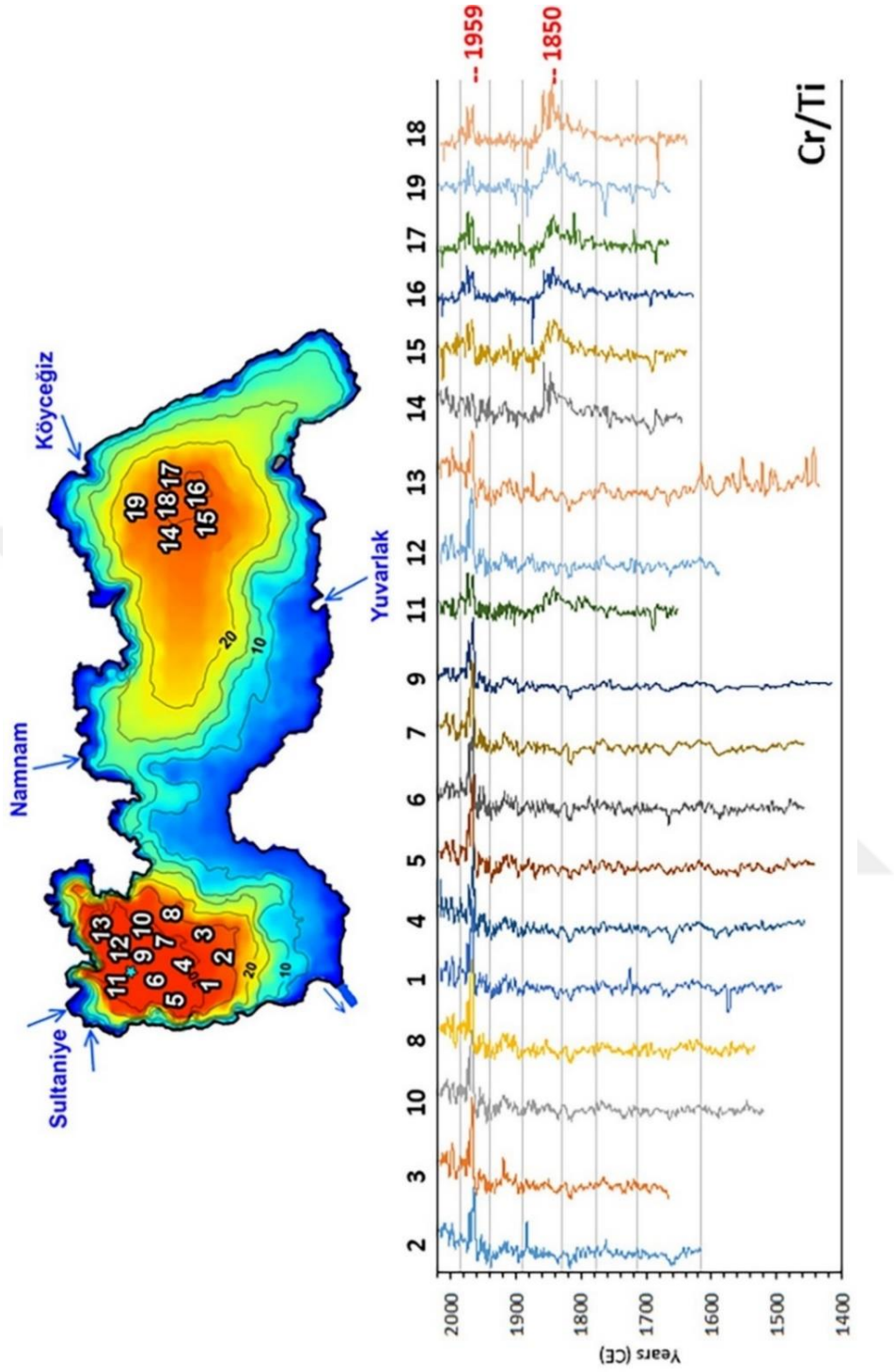

Figure 4.3. Cr/Ti peaks of correlated 19 cores and their locations in Köyceğiz lake. Blue starts indicate cores studided in Avşar et al. (2016)

4.1.2 Soft Sediment Deformation Structures (SSDS)

To better evaluate the SSDS, deformation index (DI) of SSDSs was generated and shown on 17 temporally correlated cores (Figure 4.4) It was observed that faults are generally temporally incompatible (e.g., Figure 4.4 2 faults one is in core 3 around 1900, other one in core 1 around 1915). The 1959 earthquakes (M_w 5.5-5.9) faults correlate among cores 2, 1, 12, and 17. However, it does not show consistency throughout the Köyceğiz basin cores. Cores 5, 10, 13, 14, 15, 19, and 18 recorded the 1959 earthquakes as a laminae disturbance (LD) and remained five cores do not show any distinct SSDS. The reason why 2 different modes of deformation or no deformation were detected due to the 1959 earthquake might be related to the spatial frequency of faults. Moreover, different responses of sediments to the same earthquake might be related to differences in sediment property (e.g., cohesion, particle size), the complexity of seismic waves in the basin, and basin geometry of the core location (e.g., taken from slope or basin flat). Eventhough sediments visually seem very similar, they might have some minor differences in geochemical content (e.g., carbonate content might be different). A similar situation was observed in the SSDS of the 1887 earthquake (M_w 5.8±0.5). The significant difference between the 1959 and 1887 earthquake traces is intraclast breccia, which was claimed to have the highest deformation index (Molenaar et al., 2022) detection in core 3 eventhough no deformation was observed due to the 1959 earthquake. Furthermore, no deformation was detected in any core except five cores (3, 8, 11, 12, 15). Although this clue leads to an interpretation that the complexity of seismic waves may have greater control over different modes of deformation formation, the uncertainty related to the magnitude and epicentral distance of the 1887 earthquake does not allow that. Between 1543 and 1557, chronostratigraphically correlated IBs among 3 cores were noticed, yet there are no matching AHEAD earthquakes record between these years. Between 1756 and 1851 historical earthquakes, there also exists deformations that do not correlate with any earthquakes. One possible explanation for observing these

deformations between 1543 and 1550 is that the earthquakes that triggered these deformations might be local earthquakes that were not strong enough to enter AHEAD records. Another one is earthquakes might not induce deformations only in the water-sediment interface but also in deeper parts of the stratigraphic sequences of the basin, depending on the sediments' properties. On the other hand, IBs' of 1869 (M_w 6.8±0.3) and 1756 (M_w 7.5±0.3) correlate well throughout the basin. Cores with suitable lengths to detect the 1481 (M_w 6.4±0.3) earthquake well correlate. The IB-dominated traces of the 1660 earthquake are also very compatible in each core, except cores 12 and 18. On top of each core (Figure 4.4 above the 1959 earthquake), sparse laminae disturbance was observed, which most probably occurred after the coring procedure since that part belongs to the instrumental period, and no record was found other than the 2004 earthquake, which is moderate and distant (M_w 5.3, epicentral distance approximately 40 km from the lake). Overall evaluation of this figure is, both moderate and strong earthquakes can create SSDS, most probably depending on their epicentral distances. Observation of upper-termination of faults within the core might indicate an earthquake, but the absence of it does not mean that there was no earthquake (e.g., cores 5 and 6 do not display any faults upper termination, but they show other types of deformation). This statement also emphasizes the importance of the multi-core approach in lacustrine paleoseismic investigations. IB, on the other hand, seems more reliable SSDS type since it well correlates with both earthquakes and with each other. Nevertheless, there observed IBs at some levels that do not correlate with earthquakes, but they also do not correlate with each other throughout the basin sequence. Therefore, IBs formed in the water-sediment interface seem distinguishable from the ones formed below this level. LDs also correlate with earthquakes but do not show consistency in each core as in the case of IB (e.g., Figure 4.4, 1959).

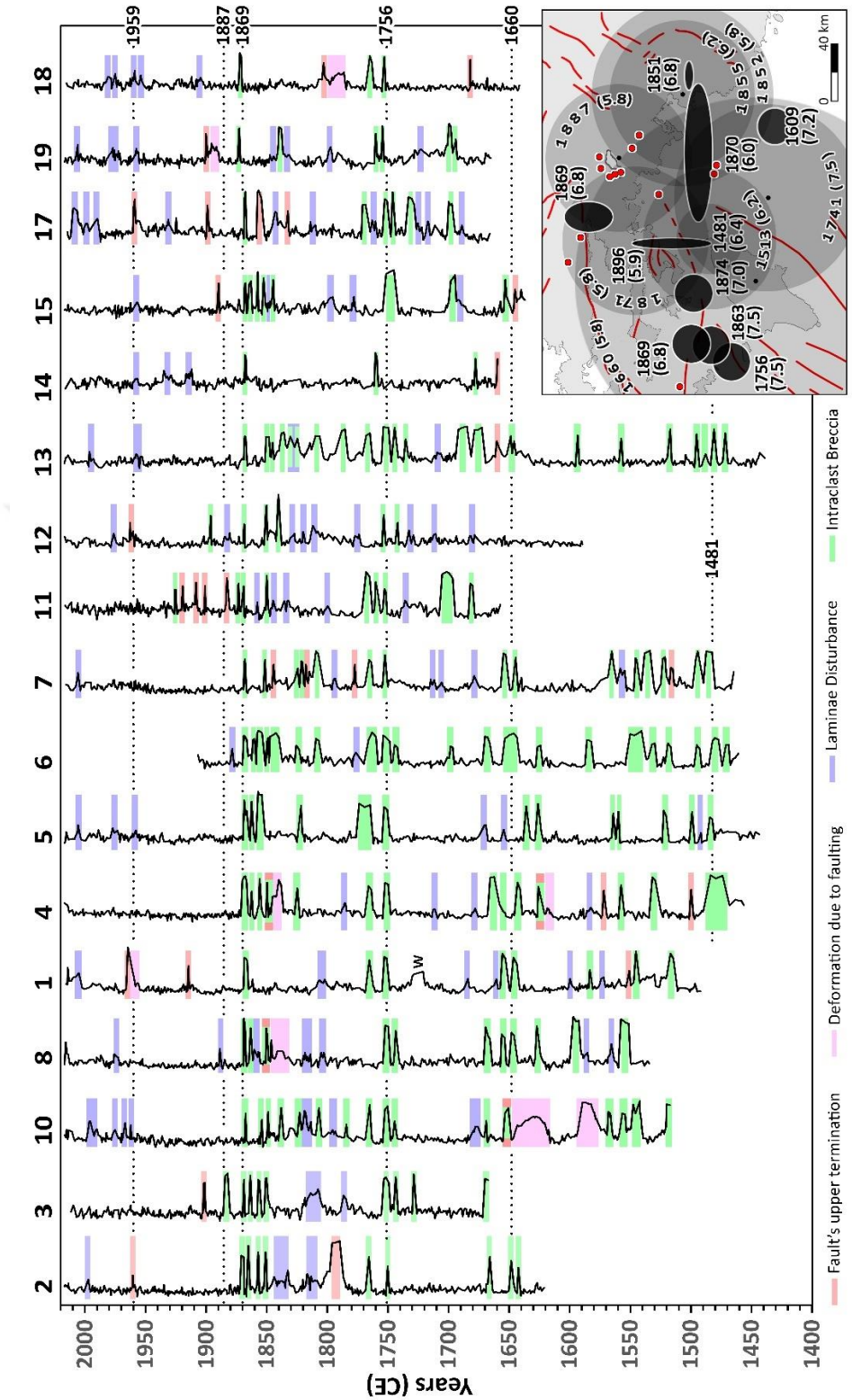

Figure 4.4. Temporal comparison of DI of 17 cores. The relation of SSDS with known earthquakes were emphasized by dashed lines with given earthquake years. Historical earthquakes were given at the bottom right corner of the figure

In order to evaluate the SSDS presented in Figure 4.4 easier, DI profiles of 17 cores and their median are overlapped in Figure 4.5 and presented together with Peak Ground Acceleration (PGA) and Peak Ground Displacement (PGD) created by the instrumental and historical period earthquakes. Cr/Ti profiles of the cores are also overlapped and presented in the same figure so that an overall evaluation of seismites in Köyceğiz sediments can be done.

Although the overlapped DI profiles look chaotic, the median DI profile, as expected, is almost blind for SSDS that are not correlating among the cores, while the SSDS correlating well are seen as distinct anomalies along the median DI profile. Temporal comparison of the median DI profile with the PGA and PGD data reveals that almost all historical earthquakes (i.e., 1869, 1851, 1852, 1855, 1756, 1741, 1660, 1609, 1513 and 1481) approximately corresponds to the significant anomalies along the median DI profile.

The most striking observation would be that the deformation related to the 1959 earthquake reported by Avşar et al. (2016), which is in fact a fault, is almost not seen in this study. Although 1959 earthquake created considerable PGA in Köyceğiz Lake and left distinct CR (i.e., Cr/Ti) traces, it did not deform the sediments much. On the countrary, it seems that the older earthquakes with much lower levels of PGAs induced more apparent SSDS. These low-PGA earthquakes seem that they created higher PGD compared to 1959 earthquake. For example, the PGA of 1756 earthquake was much lower than the PGA of 1959 earthquake, while its PGD was most probably higher than the PGD of 1959 earthquake. This observation implies that PGD might have higher control over the formation of significant SSDS than PGA. On the other hand, CR seem more relatable to PGA than PGD. The observed clustering of SSDS closer to the core bottoms seem more likely to be triggered by some local minor earthquakes, since PGD and DI correlates well in general (e.g., Figure 4.5 DI around 1750 and 1660-1600).

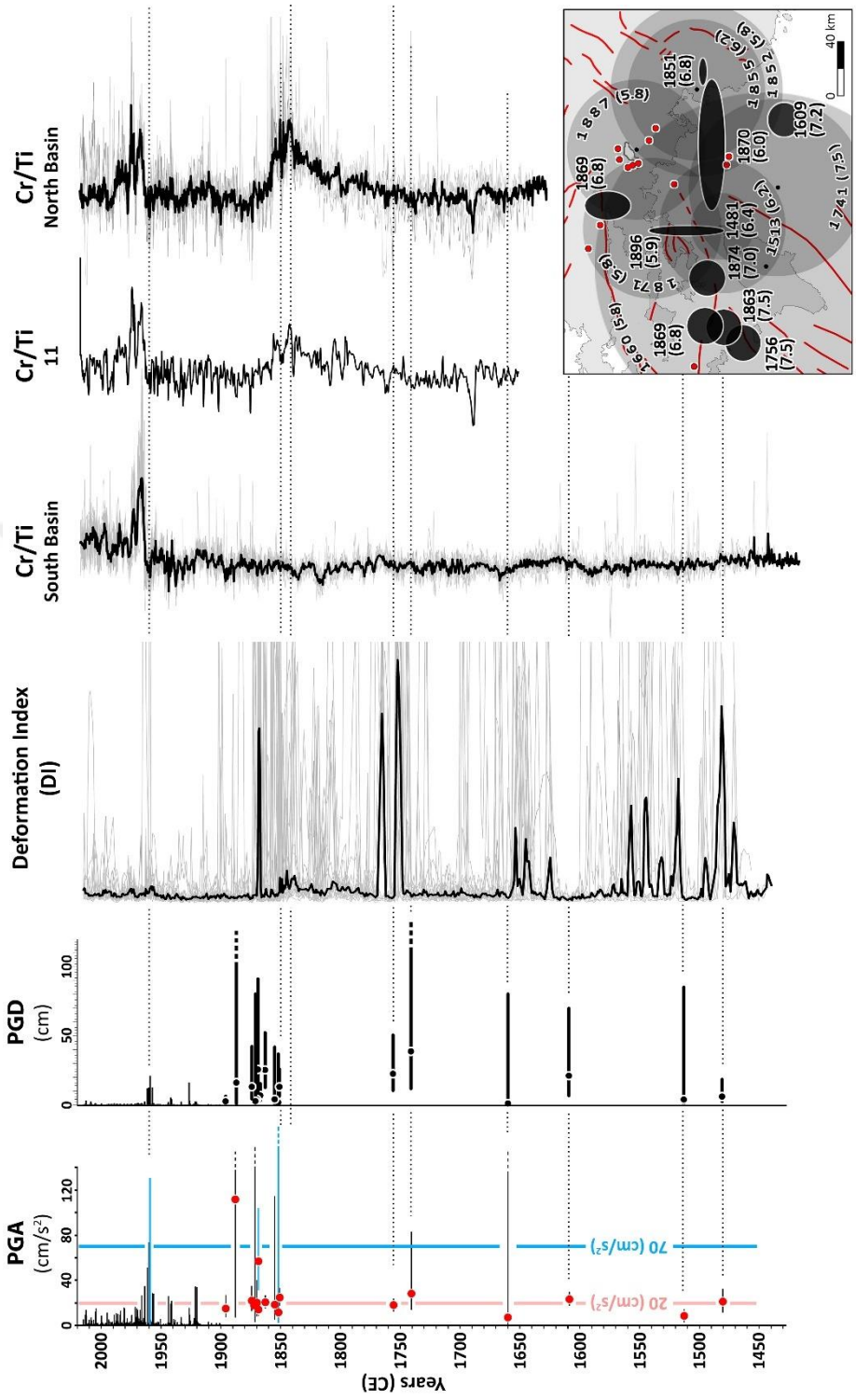

Figure 4.5. Temporal comparison of median DI profile, overlapped Cr/Ti graphs of both south and north basins cores, Cr/Ti graph of core 11, predicted PGD and PGA calculated by Avşar et al. (2016). Historical earthquakes were given at the bottom right corner of the figure

4.2 Instantaneous Deposits

Instantaneous deposits observed in the northern basin of Köyceğiz lake might have formed due to tectonic activities (mass wasting) or climatic events (floods). Turbidites are one of the most common evidence of past earthquakes that are studied in the lacustrine paleoseismology literature. However, the triggering of mass wasting due to each strong earthquake in a studied basin has been the subject of debate for a long time. Besides the strength of an earthquake, the amount of sediment influx and slope angle has a strong control over seismoturbidites and homogenite formation. For instance, it is known that the Köyceğiz basin has been shaken strong enough to create CR twice. However, homogeneous deposits haven't been observed in the southern basin, most probably due to small inlets bringing insufficient sediments to the basin. The amount of incoming sediments to the northern basin is much higher than the southern basin since larger and more streams feed it. Therefore, northern basins' homogeneous deposits were evaluated by considering differences between seismoturbidites, homogenites, and flood deposits. Homogenites were ruled out since seiche-related deformation was not observed at the bottom of the instantaneous deposits. Seismoturbidites show vertical grading due to gravitational segregation (relatively poorly sorted). In contrast, floods show lateral grading due to decreased energy away from the shoreline (relatively well-sorted). The seismoturbidites consist of particles of background sediments, while flood deposits highly consist of terrestrial sediments. Geochemical signature of these two different gradings was claimed to be also useful while distinguishing flood deposits and seismoturbidites, but basin lithology should be considered (Rapuc et al., 2022). In light of the abovementioned contrast, northern basins' instantaneous deposits were classified as flood deposits. Firstly, reworked carbonaceous laminae fragments close to the bottom of the core, as expected in turbidites, are not exist (Figure 4.6 b). Secondly, a sharp transition was observed in geochemical signals (Ca/Ti) at these homogeneous levels instead of a gravitational segregation-related gradual increase (Figure 4.6 a). The age of correlated homogeneous deposits observed on top of northern basin cores is 2012, based on varve counting. In the winter of 2012, an effective flood occurred

in the Köyceğiz district, which increased lake water enough to cause the sinkage of 2 boats. In favor of this information, event deposit in 2012 was ensured to be formed by the flood. Assigning flood to this event deposit that occurred in 2012 supports the approach when evaluating instantaneous deposits from a geochemical point of view. The slope angle of the northern basin is another supporting factor. The relatively steepest slope was calculated in the northern basin from the junction of Köyceğiz streams to core number 19. The distance between these two is approximately 1 km, and the water depth of the location of core 19 is approximately 22 m, so the corresponding slope angle is around 1.5 degrees which is too low to suscept to failure (Moernaut, 2010).

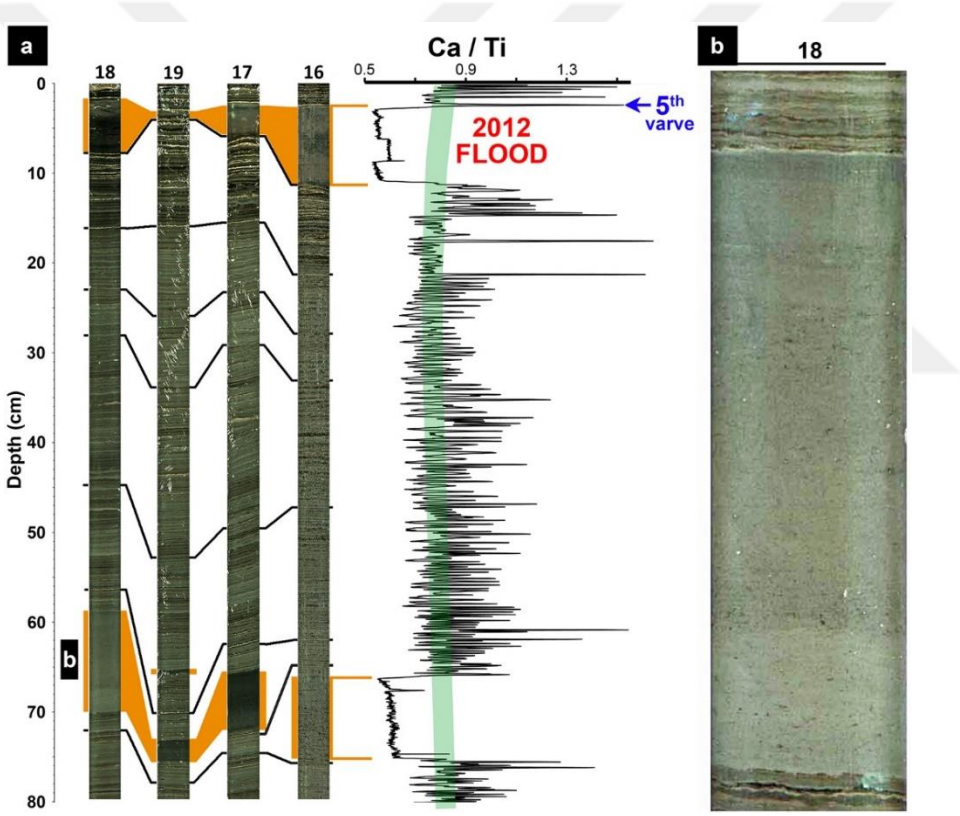

Figure 4.6. Instantaneous deposits. a) Correlated instantaneous deposits (cores 18,19,17,16) and Ca/Ti graph of core 16 (Ca/Ti background trend represented by the thick green line). b) Close-up view of the deposit in core 18.

CHAPTER 5

CONCLUSIONS

Concluding remarks of this research can be drawn as follows:

- Varve-based chronology constructed in this study reveals varve formation approximately during the last 370 and 600 years in the northern and southern basins of Köyceğiz lake, respectively.
- Eventhough Köyceğiz lake was affected by several strong earthquakes during the last 600 years, mass wasting deposits were not observed in any of the 19 cores investigated in this study. This implies mass-wasting deposits based lacustrine paleoseismic records may not completely represents the seismic history of any area under consideration, hence mass-wasting related paleoseismological interpretations should be done with care.
- Seismically amplified sediments supply from Köyceğiz catchment (CR) were distinctly detected in all of the cores just after the 1959 earthquake. On the other hand, CR related to mid-nineteenth century only detected in the cores belong to the northern basin, only in the one core from southern basin which is very close to inlets of southern basin. This observation reveals the importance of catchment size as indicated by Avsar et al., (2014).
- SSDS types observed in Köyceğiz lake are intraclast breccias (IB), faults, and laminae disturbances (LD).
- Most of the faults observed in the cores do not temporally correlate each other. Hence, absence of faulting in a core does not necessarily mean the absence of large magnitude earthquake.
- Laminae disturbances (LD) seems to be better correlated temporally compared to faults but correlation problem persists for laminae disturbances as well.

- The most common SSDS type observed in Köyceğiz lake sediments are intraclast breccias (IB). Although, inter-core correlation of IBs' is much better than faults and LDs', there are still numerous noncorrelatible IB.
- Existence of numerous noncorrelatabile SSDS in Köyceğiz sequence implies that earthquakes induce SSDS not only at the water-sediment interface but also randomly in the deeper parts of the sequence.
- Complexity in the basin-wide occurrences of SSDSs emphasizes the neccessity of multi-core investigation for more reliable lacustrine paleoseismic records
- Köyceğiz seismites record also implies that peak ground displacement (PGD), together with peak ground accelaration (PGA), may be an important parameter to induce SSDS. Although distant and big earthquakes cannot create significant PGAs, they can create significant levels of PGDs, which can induce SSDS.

REFERENCES

Agnon, A., Migowski, C., & Marco, S. (2006). Intraclast breccias in laminated sequences reviewed: Recorders of paleo-earthquakes. *Special Paper of the Geological Society of America*, *401*, 195–214. https://doi.org/10.1130/2006.2401(13)

Albini, P., Locati, M., Rovida, A., & Stucchi, M. (2013). *European Archive of Historical Earthquake Data (AHEAD). Istituto Nazionale di Geofisica e Vulcanologia (INGV).*

Alfaro, P., Delgado, J., Estévez, A., Molina, J., Moretti, M., & Soria, J. (2002). Liquefaction and fluidization structures in Messinian storm deposits (Bajo Segura Basin, Betic Cordillera, southern Spain). *International Journal of Earth Sciences*, *91*(3). https://doi.org/10.1007/s00531-001-0241-z

Allen, J. R. L. (1982). Liquidization, liquidized sediment, and the sedimentation of dense particle dispersions. In *Sedimentary structures their character and physical basis* (Vol. 2, pp. 293–241). Elsevier.

Ambraseys, N. (2009). *Earthquakes in the Mediterranean and Middle East- A multidisciplinary study of seismicity up to 1900*. Cambridge University Press.

Appleby, P. G. (2005). Chronostratigraphic Techniques in Recent Sediments. In *Tracking Environmental Change Using Lake Sediments*. https://doi.org/10.1007/0-306-47669-x_9

Avşar, U. (2013). *Lacustrine paleoseismic records from the North Anatolian Fault, Turkey* [PhD thesis]. Ghent University.

Avşar, U., Hubert-Ferrari, A., Batist, M. de, & Fagel, N. (2014). A 3400 year lacustrine paleoseismic record from the North Anatolian Fault, Turkey: Implications for bimodal recurrence behavior. *Geophysical Research Letters*, *41*(2), 377–384. https://doi.org/10.1002/2013GL058221

Avşar, U., Hubert-Ferrari, A., de Batist, M., Lepoint, G., Schmidt, S., & Fagel, N. (2014). Seismically-triggered organic-rich layers in recent sediments from Göllüköy Lake (North Anatolian Fault, Turkey). *Quaternary Science Reviews*, *103*, 67–80. https://doi.org/10.1016/j.quascirev.2014.08.020

Avşar, U., Jónsson, S., Avşar, Ö., & Schmidt, S. (2016). Earthquake-induced soft-sediment deformations and seismically amplified erosion rates recorded in varved sediments of Köyceğiz Lake (SW Turkey). *Journal of Geophysical Research: Solid Earth*, *121*(6), 4767–4779. https://doi.org/10.1002/2016JB012820

Bayarı, S. C., Kazancı, N., Koyuncu, H., Çağlar, S. S., & Gökçe, D. (1995). Determination of the origin of the waters of Köyceğiz Lake, Turkey. *Journal of Hydrology*, *166*(1–2), 171–191.

Beck, C. (2009). "Late Quaternary lacustrine paleo-seismic archives in north-western Alps: Examples of earthquake-origin assessment of sedimentary disturbances." In *Earth-Science Reviews* (Vol. 96, Issue 4, pp. 327–344). https://doi.org/10.1016/j.earscirev.2009.07.005

Becker, A., Davenport, C. A., Eichenberger, U., Gilli, E., Jeannin, P. Y., & Lacave, C. (2006). Speleoseismology: A critical perspective. In *Journal of Seismology* (Vol. 10, Issue 3). https://doi.org/10.1007/s10950-006-9017-z

Ben-Menahem, A. (1976). Dating of historical earthquakes by mud profiles of lake-bottom sediments. *Nature*, *262*(5565). https://doi.org/10.1038/262200a0

Berryman, K. R., Cochran, U. A., Clark, K. J., Biasi, G. P., Langridge, R. M., & Villamor, P. (2012). Major earthquakes occur regularly on an isolated plate boundary fault. *Science*, *336*(6089). https://doi.org/10.1126/science.1218959

Bertrand, S., Charlet, F., Chapron, E., Fagel, N., & de Batist, M. (2008). Reconstruction of the Holocene seismotectonic activity of the Southern Andes from seismites recorded in Lago Icalma, Chile, 39°S. *Palaeogeography,*

Palaeoclimatology, Palaeoecology, *259*(2–3). https://doi.org/10.1016/j.palaeo.2007.10.013

Bertrand, S., Doner, L., Ön, S. A., Sancar, U., Schudack, U., Mischke, S., Çagatay, M. N., & Leroy, S. A. G. (2011). Sedimentary record of coseismic subsidence in Hersek coastal lagoon (Izmit Bay, Turkey) and the late Holocene activity of the North Anatolian Fault. *Geochemistry, Geophysics, Geosystems*, *12*(6). https://doi.org/10.1029/2011GC003511

BİB. (2002). *Bayındırlık ve İskan bakanlığının Marmara ve Düzce depremleri sonrası faaliyetleri*. http//www.sayistay.gov.tr

Björck, S., & Wohlfarth, B. (2002). C14 chronostratigraphic techniques in paleolimnology. In W. M. Last & J. P. Smol (Eds.), *Tracking Environmental Change Using Lake Sediments. Volume 1: Basin Analysis, Coring, and Chronological Techniques* (Vol. 1, pp. 205–245). Kluwer Academic.

Björck, S., & Wohlfarth, B. (2005). 14C Chronostratigraphic Techniques in Paleolimnology. In *Tracking Environmental Change Using Lake Sediments*. https://doi.org/10.1007/0-306-47669-x_10

Boğaziçi Üniversitesi Kandilli Rasathanesi ve Deprem Araştırma Enstitüsü Bölgesel Deprem-Tsunami İzleme ve Değerlendirme Merkezi (BDTİM). (2022, November). *Türkiye ve yakın çevresindeki son depremler bölgesel deprem-tsunami izleme ve değerlendirme merkezi hızlı çözümleri*.

Bollinger, L., Tapponnier, P., Sapkota, S. N., & Klinger, Y. (2016). Slip deficit in central Nepal: omen for a repeat of the 1344 AD earthquake? *Earth, Planets and Space*, *68*(1). https://doi.org/10.1186/s40623-016-0389-1

Bommer, J. J., & Rodríguez, C. E. (2002). Earthquake-induced landslides in Central America. *Engineering Geology*, *63*(3–4). https://doi.org/10.1016/S0013-7952(01)00081-3

Caputo, R., & Helly, B. (2008). The use of distinct disciplines to investigate past earthquakes. *Tectonophysics*, *453*(1–4). https://doi.org/10.1016/j.tecto.2007.05.007

Carver, G., Plafker, G., Metz, M., Cluff, L., Slemmons, B., Johnson, E., Roddick, J., & Sorensen, S. (2004). Surface rupture on the Denali Fault interpreted from tree damage during the 1912 Delta River Mw 7.2-7.4 earthquake: Implications for the 2002 Denali Fault earthquake slip distribution. *Bulletin of the Seismological Society of America*, *94*(6 SUPPL. B). https://doi.org/10.1785/0120040625

Chapron, E., Beck, C., Pourchet, M., & Deconinck, J. F. (1999). 1822 earthquake-triggered homogenite in Lake Le Bourget (NW Alps). *Terra Nova*, *11*(2–3). https://doi.org/10.1046/j.1365-3121.1999.00230.x

Croudace, I. W., Rindby, A., & Rothwell, R. G. (2006). ITRAX: Description and evaluation of a new multi-function X-ray core scanner. *Geological Society Special Publication*, *267*. https://doi.org/10.1144/GSL.SP.2006.267.01.04

Crowell, B. W., Melgar, D., Bock, Y., Haase, J. S., & Geng, J. (2013). Earthquake magnitude scaling using seismogeodetic data. *Geophysical Research Letters*, *40*(23). https://doi.org/10.1002/2013GL058391

Dadson, S. J., Hovius, N., Chen, H., Dade, W. B., Lin, J. C., Hsu, M. L., Lin, C. W., Horng, M. J., Chen, T. C., Milliman, J., & Stark, C. P. (2004). Earthquake-triggered increase in sediment delivery from an active mountain belt. *Geology*, *32*(8). https://doi.org/10.1130/G20639.1

Daxer, C., Ortler, M., Fabbri, S. C., Hilbe, M., Hajdas, I., Dubois, N., Piechl, T., Hammerl, C., Strasser, M., & Moernaut, J. (2022). High-resolution calibration of seismically-induced lacustrine deposits with historical earthquake data in the Eastern Alps (Carinthia, Austria). *Quaternary Science Reviews*, *284*. https://doi.org/10.1016/j.quascirev.2022.107497

Daxer, C., Sammartini, M., Molenaar, A., Piechl, T., Strasser, M., & Moernaut, J. (2020). Morphology and spatio-temporal distribution of lacustrine mass-

transport deposits in wörthersee, eastern alps, Austria. In *Geological Society Special Publication* (Vol. 500, Issue 1, pp. 235–254). Geological Society of London. https://doi.org/10.1144/SP500-2019-179

Doig, R. (1990). 2300 yr history of seismicity from silting events in Lake Tadoussac, Charlevoix, Quebec. *Geology*, *18*(9). https://doi.org/10.1130/0091-7613(1990)018<0820:YHOSFS>2.3.CO;2

Doig, R. (1991). Effects of strong seismic shaking in lake sediments, and earthquake recurrence interval, Temiscaming, Quebec. *Canadian Journal of Earth Sciences*, *28*(9). https://doi.org/10.1139/e91-118

Doig, R. (1998a). 3000-year paleoseismological record from the region of the 1988 Saguenay, Quebec, earthquake. *Bulletin of the Seismological Society of America*, *88*(5). https://doi.org/10.1785/bssa0880051198

Doig, R. (1998b). Paleoseismological evidence from lake sediments for recent movement on the Denali and other faults, Yukon Territory, Canada. *Tectonophysics*, *296*(3–4). https://doi.org/10.1016/S0040-1951(98)00152-8

Doran, P. T., Berger, G. W., Lyons, W. B., Wharton, R. A., Davisson, M. L., Southon, J., & Dibb, J. E. (1999). Dating Quaternary lacustrine sediments in the McMurdo Dry Valleys, Antarctica. *Palaeogeography, Palaeoclimatology, Palaeoecology*, *147*(3–4). https://doi.org/10.1016/S0031-0182(98)00159-X

Emre Ö, Duman T Y, & Özalp S. (2011). *1:250 000 scale active fault map series of Turkey. In general directorate of mineral research and exploration.*

Fanetti, D., Anselmetti, F. S., Chapron, E., Sturm, M., & Vezzoli, L. (2008). Megaturbidite deposits in the Holocene basin fill of Lake Como (Southern Alps, Italy). *Palaeogeography, Palaeoclimatology, Palaeoecology*, *259*(2–3). https://doi.org/10.1016/j.palaeo.2007.10.014

Goldfinger, C. (2011). Submarine paleoseismology based on turbidite records. *Annual Review of Marine Science*, *3*, 35–66. https://doi.org/10.1146/annurev-marine-120709-142852

Goldfinger, C., Morey, A. E., Nelson, C. H., Gutiérrez-Pastor, J., Johnson, J. E., Karabanov, E., Chaytor, J., Eriksson, A., Winkler, M., Kalk, P., Camarero, A., Morri, C., Dunhill, G., Ramos, L., Raab, A., Pisias, N., Pourmanoutscheri, M., van Rooij, D., Amy, L., … Niemi, T. (2007). Rupture lengths and temporal history of significant earthquakes on the offshore and north coast segments of the Northern San Andreas Fault based on turbidite stratigraphy. *Earth and Planetary Science Letters*, *254*(1–2). https://doi.org/10.1016/j.epsl.2006.11.017

Goldfinger, C., Nelson, C. H., & Johnson, J. E. (2003). Holocene earthquake records from the Cascadia subduction zone and northern San Andreas fault based on precise dating of offshore turbidites. *Annual Review of Earth and Planetary Sciences*, *31*. https://doi.org/10.1146/annurev.earth.31.100901.141246

Hajdas, I., Ivy, S. D., Beer, J., Bonani, G., Imboden, D., Lotter, A. F., Sturm, M., & Suter, M. (1993). AMS radiocarbon dating and varve chronology of Lake Soppensee: 6000 to 12000 14C years BP. *Climate Dynamics*, *9*(3). https://doi.org/10.1007/BF00209748

Hall, J., Aksu, A. E., Elitez, I., Yaltirak, C., & Çifçi, G. (2014). The Fethiye-Burdur Fault Zone: A component of upper plate extension of the subduction transform edge propagator fault linking Hellenic and Cyprus Arcs, Eastern Mediterranean. *Tectonophysics*, *635*. https://doi.org/10.1016/j.tecto.2014.05.002

Heifetz, E., Agnon, A., & Marco, S. (2005). Soft sediment deformation by Kelvin Helmholtz Instability: A case from Dead Sea earthquakes. *Earth and Planetary Science Letters*, *236*(1–2), 497–504. https://doi.org/10.1016/j.epsl.2005.04.019

Hizzett, J. L., Hughes Clarke, J. E., Sumner, E. J., Cartigny, M. J. B., Talling, P. J., & Clare, M. A. (2018). Which Triggers Produce the Most Erosive, Frequent,

and Longest Runout Turbidity Currents on Deltas? *Geophysical Research Letters*, *45*(2). https://doi.org/10.1002/2017GL075751

Hovius, N., Meunier, P., Lin, C. W., Chen, H., Chen, Y. G., Dadson, S., Horng, M. J., & Lines, M. (2011). Prolonged seismically induced erosion and the mass balance of a large earthquake. *Earth and Planetary Science Letters*, *304*(3–4). https://doi.org/10.1016/j.epsl.2011.02.005

Howarth, J. D., Fitzsimons, S. J., Norris, R. J., & Jacobsen, G. E. (2012). Lake sediments record cycles of sediment flux driven by large earthquakes on the Alpine fault, New Zealand. *Geology*, *40*(12), 1091–1094. https://doi.org/10.1130/G33486.1

Howarth, J. D., Fitzsimons, S. J., Norris, R. J., & Jacobsen, G. E. (2014). Lake sediments record high intensity shaking that provides insight into the location and rupture length of large earthquakes on the Alpine Fault, New Zealand. *Earth and Planetary Science Letters*, *403*, 340–351. https://doi.org/10.1016/j.epsl.2014.07.008

Howarth, J. D., Fitzsimons, S. J., Norris, R. J., Langridge, R., & Vandergoes, M. J. (2016). A 2000 yr rupture history for the Alpine fault derived from Lake Ellery, South Island, New Zealand. *Bulletin of the Geological Society of America*, *128*(3–4), 627–643. https://doi.org/10.1130/B31300.1

I. Croudace, I. W., & Rothwell, R. G. (2015). Micro-XRF Studies of Sediment Cores: Applications of a non-destructive tool for the environmental sciences (Developments in Paleoenvironmental Research). In *Tracking Environmental Change Using Lake Sediments. Volume 2: Physical and Geochemical Methods* (Vol. 2).

Inouchi, Y., Kinugasa, Y., Kumon, F., Nakano, S., Yasumatsu, S., & Shiki, T. (1996). Turbidites as records of intense palaeoearthquakes in Lake Biwa, Japan. *Sedimentary Geology*, *104*(1–4). https://doi.org/10.1016/0037-0738(95)00124-7

Jacoby, G. C., Bunker, D. E., & Benson, B. E. (1997). Tree-ring evidence for an A.D. 1700 Cascadia earthquake in Washington and northern Oregon. *Geology*, *25*(11). https://doi.org/10.1130/0091-7613(1997)025<0999:TREFAA>2.3.CO;2

Kazanci, N., Plasa, R. H., Neubert, E., & İzbirak, A. (1992). On the limnology of lake Köycegiz (SW Anatolia). *Zoology in the Middle East*, *6*(1). https://doi.org/10.1080/09397140.1992.10637619

Keefer, D. K. (1984). Landslides caused by earthquakes. *Bulletin of the Geological Society of America*, *95*(4).

Keefer, D. K. (1994). The importance of earthquake-induced landslides to long-term slope erosion and slope-failure hazards in seismically active regions. *Geomorphology and Natural Hazards*, *10*, 265–284. https://doi.org/https://doi.org/10.1016/B978-0-444-82012-9.50022-0

Kurtuluş, T., Kurtuluş, B., Avşar, Ö., & Avşar, U. (2019). Evaluating the thermal stratification of Köyceğiz Lake (SW Turkey) using in-situ and remote sensing observations. *Journal of African Earth Sciences*, *158*. https://doi.org/10.1016/j.jafrearsci.2019.103559

Leroy, S. A. G., Boyraz, S., & Gürbüz, A. (2009). High-resolution palynological analysis in Lake Sapanca as a tool to detect recent earthquakes on the North Anatolian Fault. *Quaternary Science Reviews*, *28*(25–26). https://doi.org/10.1016/j.quascirev.2009.05.018

Leroy, S. A. G., Schwab, M. J., & Costa, P. J. M. (2010). Seismic influence on the last 1500-year infill history of Lake Sapanca (North Anatolian Fault, NW Turkey). *Tectonophysics*, *486*(1–4), 15–27. https://doi.org/10.1016/j.tecto.2010.02.005

Lotter, A. F., Merkt, J., & Strum, M. (1997). Differential sedimentation versus coring artifacts: a comparison of two widely used piston-coring methods. *Journal of Paleolimnology*, *18*, 75–85.

Lowe, D. R. (1975). Water escape structures in coarse-grained sediments. *Sedimentology*, *22*(2).

Löwemark, L., Chen, H. F., Yang, T. N., Kylander, M., Yu, E. F., Hsu, Y. W., Lee, T. Q., Song, S. R., & Jarvis, S. (2011). Normalizing XRF-scanner data: A cautionary note on the interpretation of high-resolution records from organic-rich lakes. *Journal of Asian Earth Sciences*, *40*(6). https://doi.org/10.1016/j.jseaes.2010.06.002

Malamud, B. D., Turcotte, D. L., Guzzetti, F., & Reichenbach, P. (2004). Landslides, earthquakes, and erosion. *Earth and Planetary Science Letters*, *229*(1–2). https://doi.org/10.1016/j.epsl.2004.10.018

Masson, D. G., Harbitz, C. B., Wynn, R. B., Pedersen, G., & Løvholt, F. (2006). Submarine landslides: Processes, triggers and hazard prediction. *Philosophical Transactions of the Royal Society A: Mathematical, Physical and Engineering Sciences*, *364*(1845). https://doi.org/10.1098/rsta.2006.1810

McCalpin P., J., & Nelson R., A. (2009). Introduction to Paleoseismology. In R. Dmowska, D. Hartmann, & H. T. Rossby (Eds.), *Paleoseismology* (2nd ed., Vol. 95, pp. 1–27). Elsevier.

McHugh, C. M., Kanamatsu, T., Seeber, L., Bopp, R., Cormier, M. H., & Usami, K. (2016). Remobilization of surficial slope sediment triggered by the A.D. 2011 Mw 9 Tohoku-Oki earthquake and tsunami along the Japan Trench. *Geology*, *44*(5). https://doi.org/10.1130/G37650.1

Meisling, K. E., & Sieh, K. E. (1980). Disturbance of trees by the 1857 Fort Tejon earthquake, California. *Journal of Geophysical Research*, *85*(B6). https://doi.org/10.1029/JB085iB06p03225

Mirecki, J. E. (1996). Recognition of the 1811-1812 New Madrid Earthquakes in Reelfoot Lake, Tennessee sediments using pollen data. *Journal of Paleolimnology*, *15*(2). https://doi.org/10.1007/BF00196780

Moernaut, J. (2010). *Sublacustrine landslide processes and their paleoseismological significance: Revealing the recurrence rate of giant earthquakes in South-Central Chile.* [PhD]. Ghent University.

Moernaut, J. (2020). Time-dependent recurrence of strong earthquake shaking near plate boundaries: A lake sediment perspective. In *Earth-Science Reviews* (Vol. 210). Elsevier B.V. https://doi.org/10.1016/j.earscirev.2020.103344

Moernaut, J., de Batist, M., Charlet, F., Heirman, K., Chapron, E., Pino, M., Brümmer, R., & Urrutia, R. (2007). Giant earthquakes in South-Central Chile revealed by Holocene mass-wasting events in Lake Puyehue. *Sedimentary Geology*, *195*(3–4). https://doi.org/10.1016/j.sedgeo.2006.08.005

Moernaut, J., van Daele, M., Heirman, K., Fontijn, K., Strasser, M., Pino, M., Urrutia, R., & de Batist, M. (2014). Lacustrine turbidites as a tool for quantitative earthquake reconstruction: New evidence for a variable rupture mode in south central Chile. *Journal of Geophysical Research: Solid Earth*, *119*(3), 1607–1633. https://doi.org/10.1002/2013JB010738

Moernaut, J., van Daele, M., Heirman, K., Wiemer, G., Molenaar, A., Vandorpe, T., Melnick, D., Hajdas, I., Pino, M., Urrutia, R., & de Batist, M. (2019). The subaqueous landslide cycle in south-central Chilean lakes: The role of tephra, slope gradient and repeated seismic shaking. *Sedimentary Geology*, *381*, 84–105. https://doi.org/10.1016/j.sedgeo.2019.01.002

Moernaut, J., van Daele, M., Strasser, M., Clare, M. A., Heirman, K., Viel, M., Cardenas, J., Kilian, R., Ladrón de Guevara, B., Pino, M., Urrutia, R., & de Batist, M. (2017). Lacustrine turbidites produced by surficial slope sediment remobilization: A mechanism for continuous and sensitive turbidite paleoseismic records. *Marine Geology*, *384*, 159–176. https://doi.org/10.1016/j.margeo.2015.10.009

Molenaar, A., van Daele, M., Huang, J. J. S., Strasser, M., de Batist, M., Pino, M., Urrutia, R., & Moernaut, J. (2022). Disentangling factors controlling

earthquake-triggered soft-sediment deformation in lakes. *Sedimentary Geology*, *438*. https://doi.org/10.1016/j.sedgeo.2022.106200

Molenaar, A., van Daele, M., Vandorpe, T., Degenhart, G., de Batist, M., Urrutia, R., Pino, M., Strasser, M., & Moernaut, J. (2021). What controls the remobilization and deformation of surficial sediment by seismic shaking? Linking lacustrine slope stratigraphy to great earthquakes in South–Central Chile. *Sedimentology*, *68*(6), 2365–2396. https://doi.org/10.1111/sed.12856

Molina, J. M., Alfaro, P., Moretti, M., & Soria, J. M. (1998). Soft-sediment deformation structures induced by cyclic stress of storm waves in tempestites (Miocene, Guadalquivir Basin, Spain). *Terra Nova*, *10*(3). https://doi.org/10.1046/j.1365-3121.1998.00183.x

Monecke, K., Anselmetti, F. S., Becker, A., Schnellmann, M., Sturm, M., & Giardini, D. (2006). Earthquake-induced deformation structures in lake deposits: A Late Pleistocene to Holocene paleoseismic record for Central Switzerland. *Eclogae Geologicae Helvetiae*, *99*(3). https://doi.org/10.1007/s00015-006-1193-x

Monecke, K., Anselmetti, F. S., Becker, A., Sturm, M., & Giardini, D. (2004). The record of historic earthquakes in lake sediments of Central Switzerland. *Tectonophysics*, *394*(1–2). https://doi.org/10.1016/j.tecto.2004.07.053

Mook, W. G. (1986). Recommendations/resolutions adopted by the 12th International Radiocarbon Conference. *Radiocarbon*, *28*.

Moretti, M., & Sabato, L. (2007). Recognition of trigger mechanisms for soft-sediment deformation in the Pleistocene lacustrine deposits of the Sant'Arcangelo Basin (Southern Italy): Seismic shock vs. overloading. *Sedimentary Geology*, *196*(1–4), 31–45. https://doi.org/10.1016/j.sedgeo.2006.05.012

Moretti, M., Soria, J. M., Alfaro, P., & Walsh, N. (2001). Asymmetrical soft-sediment deformation structures triggered by rapid sedimentation in turbiditic

deposits (late miocene,guadix basin, Southern Spain). *Facies*, *44*. https://doi.org/10.1007/bf02668179

Nichols, R. J., Sparks, R. S. J., & Wilson, C. J. N. (1994). Experimental studies of the fluidization of layered sediments and the formation of fluid escape structures. *Sedimentology*, *41*(2), 233–253. https://doi.org/https://doi.org/10.1111/j.1365-3091.1994.tb01403.x

Obermeier, S. F. (1996). Use of liquefaction-induced features for paleoseismic analysis - An overview of how seismic liquefaction features can be distinguished from other features and how their regional distribution and properties of source sediment can be used to infer the location and strength of Holocene paleo-earthquakes. *Engineering Geology*, *44*(1–4). https://doi.org/10.1016/s0013-7952(96)00040-3

Ojala, A. E. K., & Tiljander, M. (2003). Testing the fidelity of sediment chronology: Comparison of varve and paleomagnetic results from Holocene lake sediments from central Finland. *Quaternary Science Reviews*, *22*(15–17). https://doi.org/10.1016/S0277-3791(03)00140-9

Oliveira, C. M. M., Hodgson, D. M., & Flint, S. S. (2009). Aseismic controls on in situ soft-sediment deformation processes and products in submarine slope deposits of the Karoo Basin, South Africa. *Sedimentology*, *56*(5). https://doi.org/10.1111/j.1365-3091.2008.01029.x

Oswald, P., Strasser, M., Hammerl, C., & Moernaut, J. (2021). Seismic control of large prehistoric rockslides in the Eastern Alps. *Nature Communications*, *12*(1). https://doi.org/10.1038/s41467-021-21327-9

Owen, G. (1987). Deformation processes in unconsolidated sands. *Geological Society Special Publication*, *29*. https://doi.org/10.1144/GSL.SP.1987.029.01.02

Owen, G. (2003). Load structures: Gravity-driven sediment mobilization in the shallow subsurface. *Geological Society Special Publication*, *216*. https://doi.org/10.1144/GSL.SP.2003.216.01.03

Owen, G., & Moretti, M. (2011). Identifying triggers for liquefaction-induced soft-sediment deformation in sands. *Sedimentary Geology*, *235*(3–4), 141–147. https://doi.org/10.1016/j.sedgeo.2010.10.003

Özalp, S., & Kürçer, A. (2022). *23 Kasım Gölyaka (Düzce) depremi (Mw 6,0) saha gözlemleri ve değerlendirme raporu*.

Rapuc, W., Arnaud, F., Sabatier, P., Anselmetti, F. S., Piccin, A., Peruzza, L., Bastien, A., Augustin, L., Régnier, E., Gaillardet, J., & von Grafenstein, U. (2022). Instant sedimentation in a deep Alpine lake (Iseo, Italy) controlled by climate, human and geodynamic forcing. *Sedimentology*, *69*(4), 1816–1840. https://doi.org/10.1111/sed.12972

Ringrose, P. S. (1989). Palaeoseismic (?) liquefaction event in late Quaternary lake sediment at Glen Roy, Scotland. *Terra Nova*, *1*(1). https://doi.org/10.1111/j.1365-3121.1989.tb00326.x

Rodríguez, C. E., Bommer, J. J., & Chandler, R. J. (1999). Earthquake-induced landslides: 1980-1997. *Soil Dynamics and Earthquake Engineering*, *18*(5). https://doi.org/10.1016/S0267-7261(99)00012-3

Rodríguez-Pascua, M. A., Calvo, J. P., de Vicente, G., & Gómez-Gras, D. (2000). Soft-sediment deformation structures interpreted as seismites in lacustrine sediments of the Prebetic Zone, SE Spain, and their potential use as indicators of earthquake magnitudes during the Late Miocene. *Sedimentary Geology*, *135*(1–4), 117–135. https://doi.org/https://doi.org/10.1016/S0037-0738(00)00067-1

Rothwell, R. G., Hoogakker, B., Thomson, J., Croudace, I. W., & Frenz, M. (2006). Turbidite emplacement on the southern Balearic Abyssal Plain (western Mediterranean Sea) during Marine Isotope Stages 1-3: An application of

ITRAX XRF scanning of sediment cores to lithostratigraphic analysis. *Geological Society Special Publication*, *267*. https://doi.org/10.1144/GSL.SP.2006.267.01.06

Sakellariou, D., & Tsampouraki-Kraounaki, K. (2018). Plio-quaternary extension and strike-slip tectonics in the aegean. In *Transform Plate Boundaries and Fracture Zones* (pp. 339–374). Elsevier. https://doi.org/10.1016/B978-0-12-812064-4.00014-1

Sammartini, M., Moernaut, J., Anselmetti, F. S., Hilbe, M., Lindhorst, K., Praet, N., & Strasser, M. (2019). An atlas of mass-transport deposits in lakes. In *Submarine Landslides: Subaqueous Mass Transport Deposits from Outcrops to Seismic Profiles* (pp. 201–226). Wiley. https://doi.org/10.1002/9781119500513.ch13

Schnellmann, M., Anselmetti, F. S., Giardini, D., & McKenzie, J. A. (2005). Mass movement-induced fold-and-thrust belt structures in unconsolidated sediments in Lake Lucerne (Switzerland). *Sedimentology*, *52*(2). https://doi.org/10.1111/j.1365-3091.2004.00694.x

Schnellmann, M., Anselmetti, F. S., Giardini, D., & McKenzie, J. A. (2006). 15,000 Years of mass-movement history in Lake Lucerne: Implications for seismic and tsunami hazards. *Eclogae Geologicae Helvetiae*, *99*(3). https://doi.org/10.1007/s00015-006-1196-7

Seilacher, A. (1969). Fault-graded beds interpreted as seismites. *Sedimentology*, *13*(1–2). https://doi.org/https://doi.org/10.1111/j.1365-3091.1969.tb01125.x

Şenel, M. (1997). Geological map series of Turkey 1:100 000 scale No.1, Geological map of Fethiye L7 quadrangle. In *General directorate of mineral research and exploration, Geological research departmentt*.

Shanmugam, G. (2017). Global case studies of soft-sediment deformation structures (SSDS): Definitions, classifications, advances, origins, and problems. *Journal of Palaeogeography*, *6*(4). https://doi.org/10.1016/j.jop.2017.06.004

Shotton, F. W. (1972). An example of hard-water error in radiocarbon dating of vegetable matter. *Nature*, *240*(5382). https://doi.org/10.1038/240460a0

Strasser, M., Monecke, K., Schnellmann, M., & Anselmetti, F. S. (2013a). Lake sediments as natural seismographs: A compiled record of Late Quaternary earthquakes in Central Switzerland and its implication for Alpine deformation. *Sedimentology*, *60*(1), 319–341. https://doi.org/10.1111/sed.12003

Strasser, M., Monecke, K., Schnellmann, M., & Anselmetti, F. S. (2013b). Lake sediments as natural seismographs: A compiled record of Late Quaternary earthquakes in Central Switzerland and its implication for Alpine deformation. *Sedimentology*, *60*(1), 319–341. https://doi.org/10.1111/sed.12003

Thomson, J., Croudace, I. W., & Rothwell, R. G. (2006). A geochemical application of the ITRAX scanner to a sediment core containing eastern Mediterranean sapropel units. *Geological Society Special Publication*, *267*. https://doi.org/10.1144/GSL.SP.2006.267.01.05

Tosun, L., Avşar, U., Avşar, Ö., Dondurur, D., & Kaymakcı, N. (2021). Active tectonics and kinematics of Fethiye-Göcek Bay, SW Turkey: Insight about the eastern edge of Pliny-Strabo Trenches. *Journal of Structural Geology*, *145*. https://doi.org/10.1016/j.jsg.2021.104287

Turner, G. M., & Thompson, R. (1981). Lake sediment record of the geomagnetic secular variation in Britain during Holocene times. *Geophysical Journal of the Royal Astronomical Society*, *65*(3). https://doi.org/10.1111/j.1365-246X.1981.tb04879.x

Urgeles, R., & Camerlenghi, A. (2013). Submarine landslides of the Mediterranean Sea: Trigger mechanisms, dynamics, and frequency-magnitude distribution. *Journal of Geophysical Research: Earth Surface*, *118*(4). https://doi.org/10.1002/2013JF002720

van Daele, M., Haeussler, P. J., Witter, R. C., Praet, N., & de Batist, M. (2019). The sedimentary record of the 2018 Anchorage earthquake in Eklutna Lake, Alaska:

Calibrating the lacustrine seismograph. *Seismological Research Letters*, *91*(1), 126–141. https://doi.org/10.1785/0220190204

Vandekerkhove, E., van Daele, M., Praet, N., Cnudde, V., Haeussler, P. J., & de Batist, M. (2020). Flood-triggered versus earthquake-triggered turbidites: A sedimentological study in clastic lake sediments (Eklutna Lake, Alaska). *Sedimentology*, *67*(1), 364–389. https://doi.org/10.1111/sed.12646

Vologina, E. G., Kalugin, I. A., Osukhovskaya, Y. N., Sturm, M., Ignatova, N. v., Radziminovich, Y. B., Dar'in, A. v., & Kuz'min, M. I. (2010). Sedimentation in Proval Bay (Lake Baikal) after earthquake-induced subsidence of part of the Selenga River delta. *Russian Geology and Geophysics*, *51*(12). https://doi.org/10.1016/j.rgg.2010.11.008

Waldmann, N., Anselmetti, F. S., Ariztegui, D., Austin, J. A., Pirouz, M., Moy, C. M., & Dunbar, R. (2011). Holocene mass-wasting events in Lago Fagnano, Tierra del Fuego (54°S): Implications for paleoseismicity of the Magallanes-Fagnano transform fault. *Basin Research*, *23*(2). https://doi.org/10.1111/j.1365-2117.2010.00489.x

Wang, J., Jin, Z., Hilton, R. G., Zhang, F., Densmore, A. L., Li, G., & Joshua West, A. (2015). Controls on fluvial evacuation of sediment from earthquake-triggered landslides. *Geology*, *43*(2), 115–118. https://doi.org/10.1130/G36157.1

Wetzler, N., Marco, S., & Heifetz, E. (2010). Quantitative analysis of seismogenic shear-induced turbulence in lake sediments. *Geology*, *38*(4), 303–306. https://doi.org/10.1130/G30685.1

Yanites, B. J., Tucker, G. E., Mueller, K. J., & Chen, Y. G. (2010). How rivers react to large earthquakes: Evidence from central Taiwan. *Geology*, *38*(7). https://doi.org/10.1130/G30883.1

Zolitschka, B., Francus, P., Ojala, A. E. K., & Schimmelmann, A. (2015). Varves in lake sediments - a review. In *Quaternary Science Reviews* (Vol. 117, pp. 1–41). Elsevier Ltd. https://doi.org/10.1016/j.quascirev.2015.03.019

APPENDICES

APPENDIX -1

High-resolution version of this image is provided as print-out attached to hardcover.

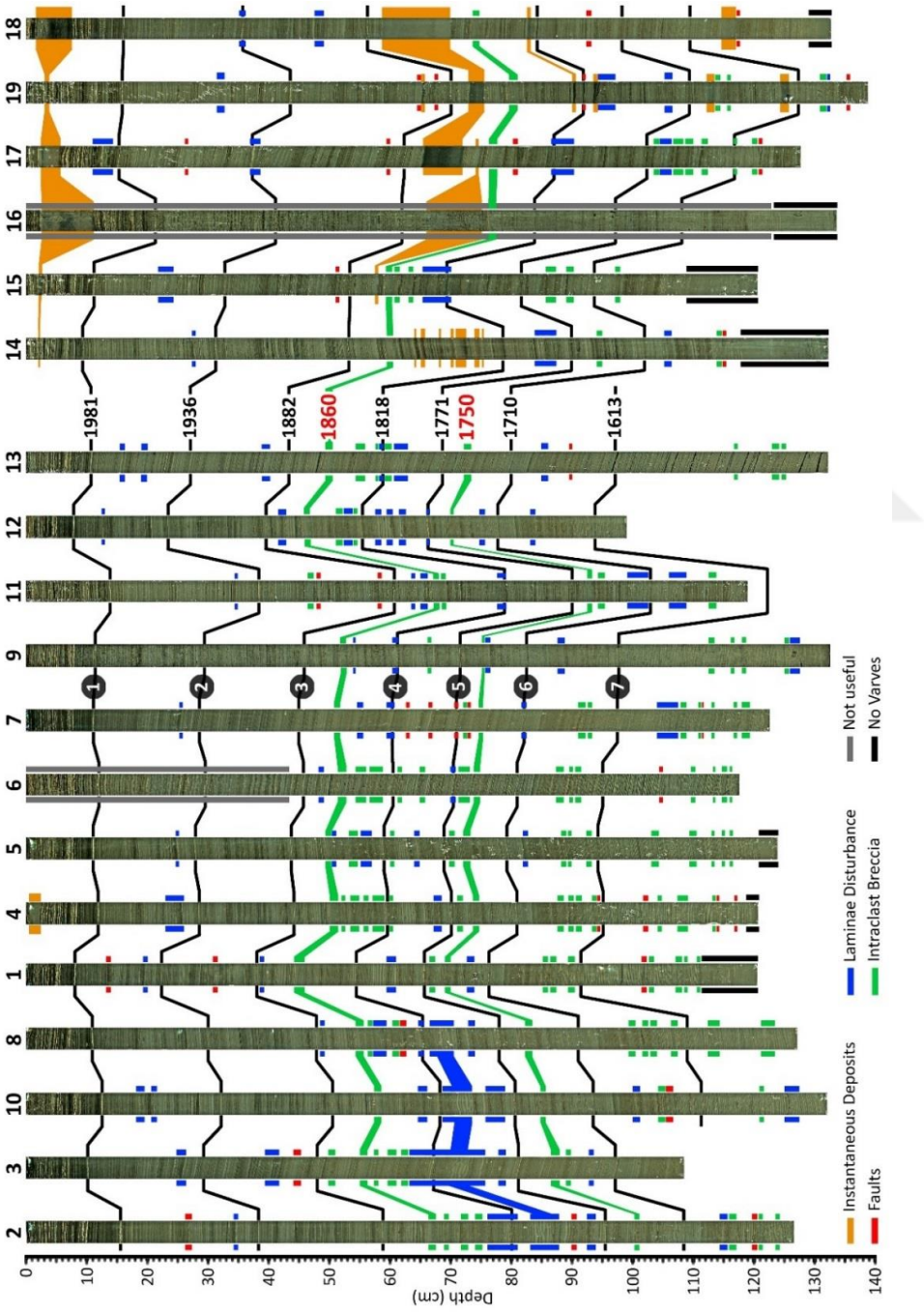

APPENDIX -2

High-resolution version of this image is provided as print-out attached tohardcover.

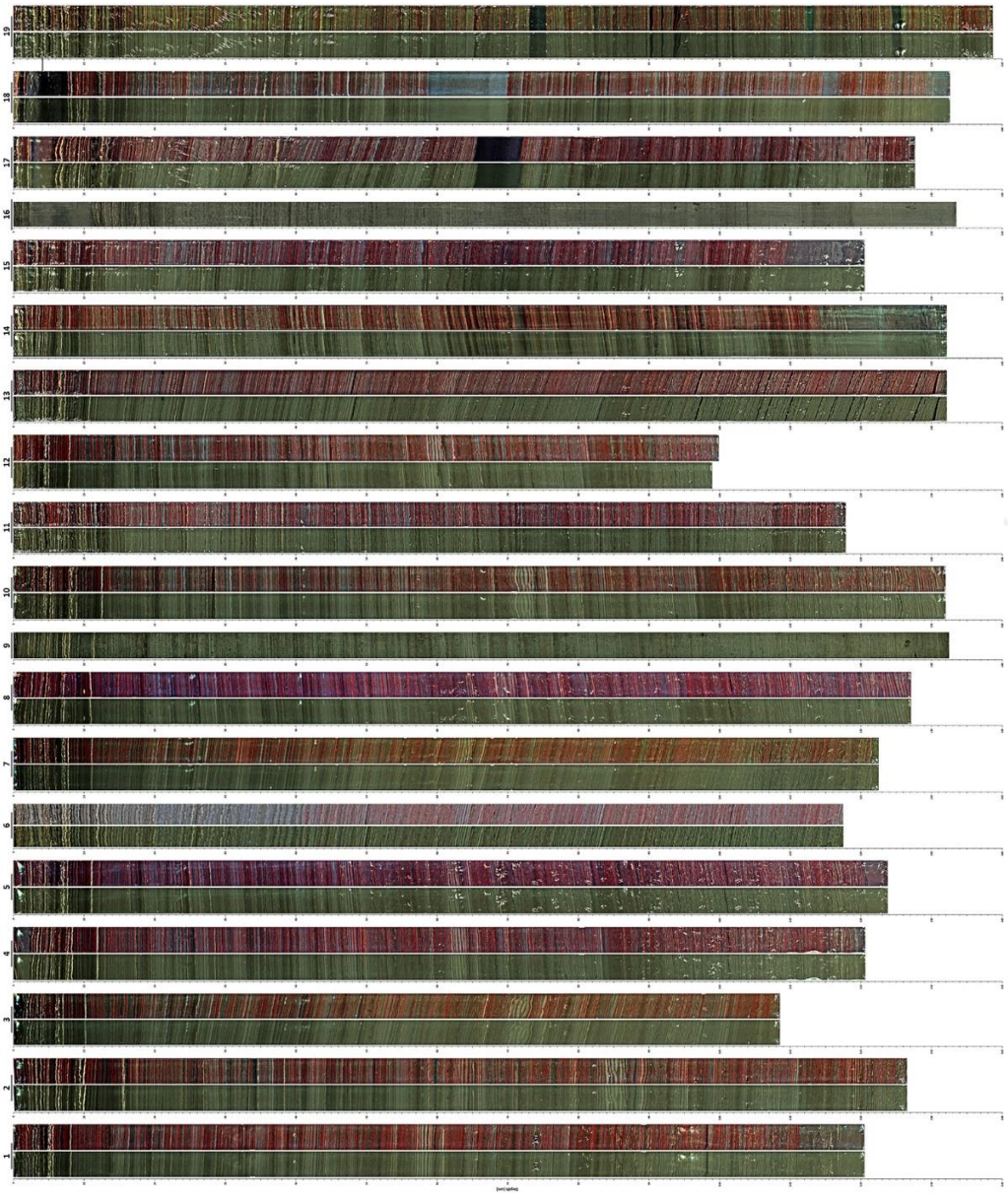

APPENDIX - 1

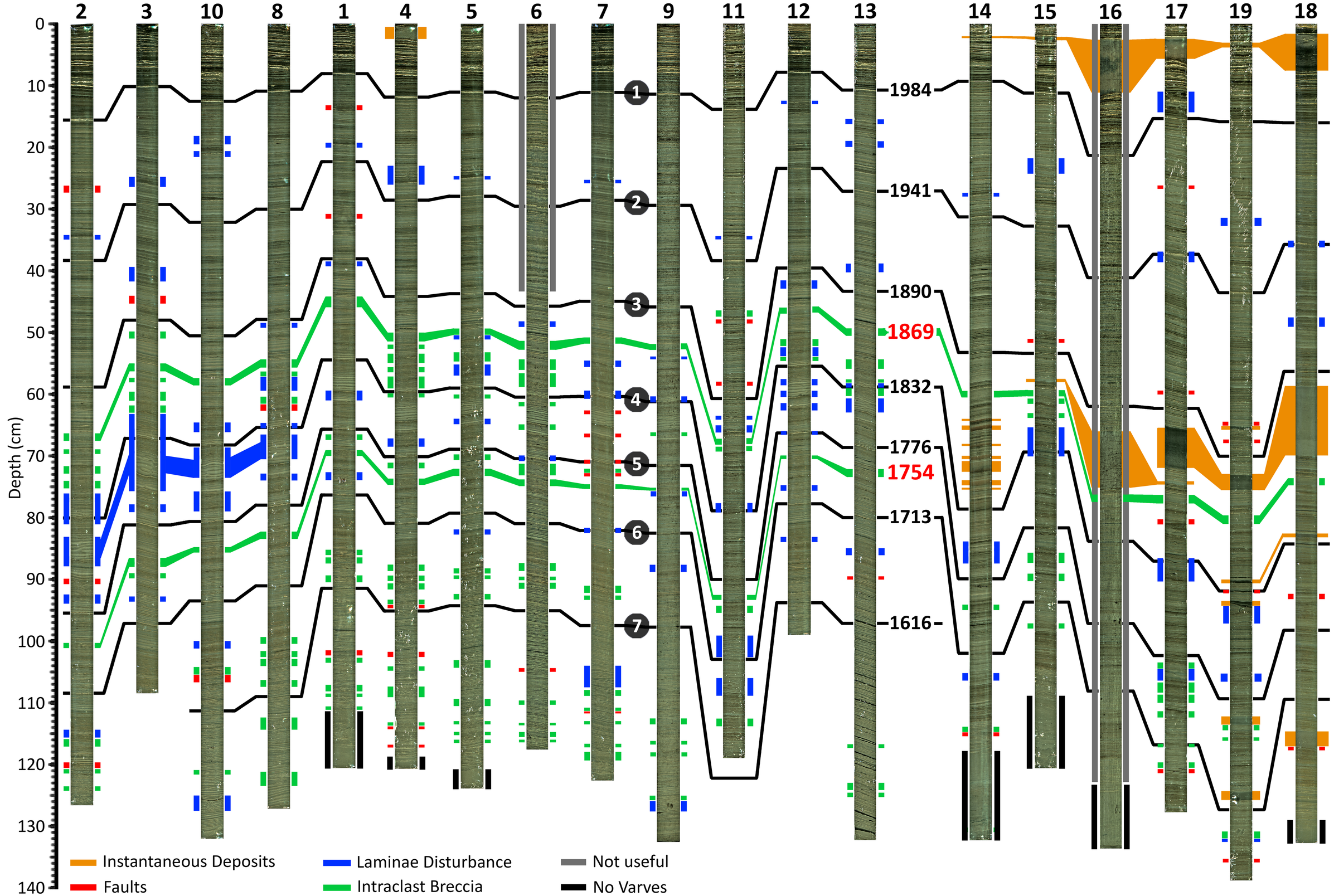
2
3
10
8
1
4
5
6
7
9
11
12
13
14
15
16
17
19
18
0
10
20
30
40
50
60
70
80
90
100
110
120
130
140
Depth (cm)
1
2
3
4
5
6
7
1984
1941
1890
1869
1832
1776
1754
1713
1616
Instantaneous Deposits
Faults
Laminae Disturbance
Intraclast Breccia
Not useful
No Varves

APPENDIX - 2

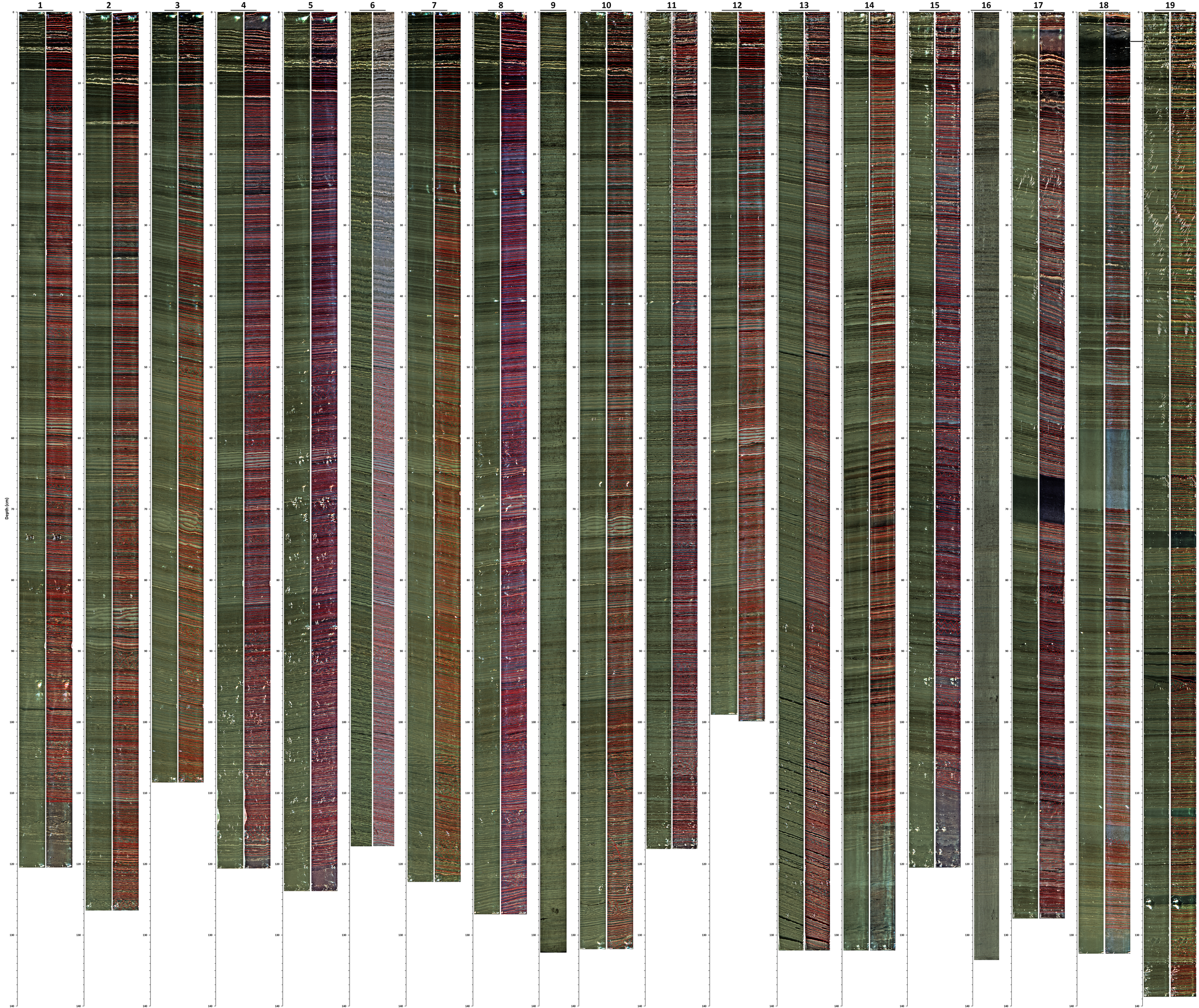
1
2
3
4
5
6
7
8
9
10
11
12
13
14
15
16
17
18
19
Depth (cm)
0
10
20
30
40
50
60
70
80
90
100
110
120
130
140